Synergistic Application of Advanced Machine Learning and Computer Vision Techniques for the Detection of Exoplanet and Star: Leveraging Contrastive Learning in Astronomical Imagery

by

Ashraful Kabir Alif
20301227
Sk Jamil Hossain
20301261
Md Impreeaj Hossain
20341031
Shihab Shahriar Antor
20301113
Arghya Pranto Roy
20201210

A thesis submitted to the Department of Computer Science and Engineering
in partial fulfillment of the requirements for the degree of
B.Sc. in Computer Science

Department of Computer Science and Engineering
Brac University
November 2024

Declaration

It is hereby declared that

1. The thesis submitted is my/our own original work while completing degree at Brac University.

2. The thesis does not contain material previously published or written by a third party, except where this is appropriately cited through full and accurate referencing.

3. The thesis does not contain material which has been accepted, or submitted, for any other degree or diploma at a university or other institution.

4. We have acknowledged all main sources of help.

Student's Full Name & Signature:

Ashraful Kabir Alif
20301227

Sk Jamil Hossain
20301261

Md Impreeaj Hossain
20341031

Shihab Shahriar Antor
20301113

Arghya Pranto Roy
20201210

Approval

The thesis titled "Synergistic Application of Advanced Machine Learning and Computer Vision Techniques for the Detection of Exoplanet and Star: Leveraging Contrastive Learning in Astronomical Imagery " submitted by

1. Ashraful Kabir Alif(20301227)
2. Sk Jamil Hossain(20301261)
3. Md Impreeaj Hossain(20341031)
4. Shihab Shahriar Antor(20301113)
5. Arghya Pranto Roy(20201210)

Of Summer, 2024 has been accepted as satisfactory in partial fulfillment of the requirement for the degree of B.Sc. in Computer Science on October 17, 2024.

Examining Committee:

Supervisor:
(Member)

Md. Golam Rabiul Alam, PhD
Professor
Department of Computer Science and Engineering
Brac University

Thesis Coordinator:
(Chair)

Md. Golam Rabiul Alam, PhD
Professor
Department of Computer Science and Engineering
Brac University

Head of Department:
(Chair)

Sadia Hamid Kazi, PhD
Chairperson and Associate Professor
Department of Computer Science and Engineering
Brac University

Abstract

The detection of exoplanets through direct imaging has become increasingly feasible with the advent of modern telescopes like the James Webb Space Telescope (JWST) and its MIRI coronagraph. These instruments have significantly expanded the availability of high-quality direct imaging datasets, offering new opportunities for astronomical research. However, despite these advances, traditional machine learning methods, such as Convolutional Neural Networks (CNNs) and Graph Neural Networks (GNNs), face limitations when applied to exoplanet detection. These limitations include difficulties in detecting exoplanets that are faint and often obscured by the bright light of nearby stars, as well as challenges posed by small and imbalanced datasets. To address these challenges, this thesis introduces a novel machine learning approach that leverages contrastive learning and few-shot learning. Contrastive learning is used to improve the distinguishing ability of the model focusing on separating different celestial objects such as exoplanets and stars. It learns representations that distinguish between these objects despite the high noise, low contrast and complex nature of astronomical images. In addition, to address the problem of few training images, the approach called few-shot learning is used to achieve good results even when only a few pixel-labeled images of exoplanets are available. The components of the proposed framework include integration of contrastive learning with ResNet18 and Siamese Networks followed by experimenting with two YOLO models. The decision to increase the model's complexity going to provide higher accuracy over the simple method in processing noise contexts or in the limited availability of exoplanet instances. Through the sophisticated learning methodologies presented in this work, our model achieved an accuracy of 92.16%, significantly enhancing detection capabilities. By utilizing YOLOv5, our approach also achieved high performance in Dice Coefficient (1.0 for star and 0.9 for exoplanet) and Intersection over Union (IoU) metrics (1.0 for star and 0.8 for exoplanet), underscoring the model's effectiveness in direct imaging exoplanet detection. This advancement not only contributes to current astronomy efforts but also enables more powerful discoveries in the future.

Keywords: Exoplanet detection, direct imaging, James Webb Space Telescope (JWST), MIRI coronagraph, machine learning, contrastive learning, few-shot learning, Convolutional Neural Networks (CNNs), Graph Neural Networks (GNNs), Siamese Networks, YOLOv5, YOLOv7, astronomical imagery, celestial object classification, ResNet18.

Acknowledgement

Firstly, all praise to the Great Allah for whom our thesis have been completed without any major interruption.Secondly, to our supervisor Dr. Md. Golam Rabiul Alam sir for his kind support and advice in our work. He helped us whenever we needed help.Thirdly, Md. Tanzim Reza sir supported us, and Dr. Md. Ashraful Alam sir and his panel provided reviews that greatly helped us in our later works. Finally to our parents without their throughout support it may not be possible. With their kind support and prayer we are now on the verge of our graduation.

Table of Contents

List of Figures

List of Tables

Nomenclature

The next list describes several symbols & abbreviation that will be later used within the body of the document

AstroImageJ A software used for astronomical image processing, particularly for pre-processing FITS files

Coronagraphic Imaging A technique used to block out the bright light from stars to better detect the surrounding exoplanets

Exoplanet A planet that orbits a star outside the solar system

$F2300C$ A specific filter used by MIRI to isolate infrared wavelengths for better exoplanet detection

FITS Flexible Image Transport System format, a standard data format used for astronomical data

JWST James Webb Space Telescope, a space telescope used for astronomical observations

$LYOT$_2300 Another filter used with the MIRI instrument for coronagraphic imaging

MIRI Mid-Infrared Instrument on the JWST, used for detecting exoplanets and stars through coronagraphic imaging

Chapter 1

Introduction

Exoplanet detection has long been a cornerstone of astronomical research, providing insights into planets beyond our solar system and their potential for habitability. Historically, exoplanet detection relied on indirect methods like transit photometry and radial velocity due to the lack of direct imaging capabilities. However, the recent advancements in space-based telescopes, particularly the James Webb Space Telescope (JWST) and its MIRI coronagraph, have enabled the capture of high-quality direct images of exoplanets and their host stars. These advancements have created a unique opportunity to leverage large datasets of direct imaging for machine learning applications.Despite the availability of these images, the task of detecting exoplanets remains challenging. Exoplanets often appear as dim objects located near much brighter stars, making their detection difficult even in high-resolution images. Traditional machine learning approaches, such as Convolutional Neural Networks (CNNs) and Graph Neural Networks (GNNs), have been employed to enhance detection, but limitations persist in terms of accuracy and generalization due to the faint and complex nature of the data.

This thesis aims to address these challenges by employing advanced machine learning techniques, such as contrastive learning and few-shot learning, to improve the detection of exoplanets in direct imaging data. The following sections outline the specific problem this thesis addresses and the objectives it seeks to achieve.

1.1 Problem Statement

Detecting exoplanets which are planets outside our solar system, is a significant scientific discovery that helps us understand the universe better. While various methods like the transit method and radial velocity have successfully discovered many exoplanets, direct imaging has faced notable challenges. Traditional techniques such as coronagraphy, starshade, and adaptive optics are limited by their inability to adequately separate the light of exoplanets from the overwhelming brightness of their host stars. This has resulted in the detection of only a few exoplanets through direct Imaging.

With the help of subsequent improved telescopes like the James Webb Space Telescope (JWST) and its MIRI coronagraph it has become possible to obtain high quality direct images of exoplanets and stars. Modern technological developments have generated an immense volume of direct imaging information: it remains an uncharted area. But yet, the direct imaging of exoplanets is still not an easy job. Transiting exoplanets are typically low signal to noise candidates that are indistinguishable from stars in terms of brightness and appearance. Several advances of Machine learning classifiers have been used in the past to improve detection processes, including CNN and GNN. Being based on these models the results have appeared promising for classification and detection of exoplanets, however, such models are restricted for direct imaging data because of such factors as low brightness of exoplanets and high scatter of images. In response to these challenges, this thesis presents an innovative solution through the use of a state of the art machine learning methodologies such as contrastive learning and few-shot learning. These methods are meant to increase the amounts of detected cases by models, particularly in situations when data is sparse or severely unbalanced. Overall, this research intends to apply the contrastive learning into the improvement of ResNet18, and Siamese network with an intention of increasing the detection of stars and exoplanets in cases of noisy and limited data.

1.2 Research Contributions

The aim of this thesis is to develop a efficient machine learning framework that significantly improves the detection of exoplanets from direct imaging data by utilizing techniques such as contrastive learning and few-shot learning. This Research address the challenges faced by traditional exoplanet detection methods, such as coronagraphy and starshades, which often struggle to detect faint exoplanets close to their host stars due to the overwhelming brightness of the star. The Contributions are as follows:

- We introduced a Contrastive Learning Approach which implement contrastive learning to improve the model's ability to differentiate between celestial objects, particularly exoplanets and stars, in complex, noisy images. This Contrastive Learning Architecture works well for the dataset we have used.

- Incorporate few-shot learning techniques to address the challenge of limited exoplanet data by enabling the model to generalize well from a small number of examples.

- We have applied YOLOv5 and YOLOv7 for the detection model that not only identifies exoplanets but also accurately locates them in direct imaging data, accounting for their faint and dim nature in the presence of nearby stars.

- Extensive Simulations on well known dataset, JWST MIRI coronagraph[36] demonstrate the learning performance (i.e., 92.16% generalization) of the proposed approach which is our Contrastive Learning architecture. Simulation result depict significant gain in system performance of 0.17% as compared to the base line; and hence, ensuring low-latency model aggregation or fast knowledge acquisition.

1.3 Report Organization

The rest of this paper is structured as follows. Section 2 provides details on the different methods used for exoplanet detection and machine learning approaches for this detection. Section 3 outlines the methodology of our proposed model in detail. Section 4 discusses the performance evaluation metrics of different models along with our proposed model. Lastly Section 5 concludes the paper.

Chapter 2

Literature Review

The discovery of exoplanets, planets orbiting stars outside our solar system, has enabled us to learn a new range of things about the universe. Since then, several methods of detection have emerged; each helping to move the search for distant worlds into the future. These traditional approaches like the Transit Method and Radial Velocity (RV) Method have been key in early discoveries of exoplanets, especially through Kepler and TESS. More precision in detection and analysis of nuclear materials is made possible by modern techniques which incorporate machine learning (ML) algorithms as data complexity increases. Fortunately, planets that might have otherwise gone undetected have been newly found with Complementary methods such as Direct Imaging, Astrometry, and Gravitational Microlensing. This literature review discusses the evolution of detection of exoplanets with these methods, with an emphasis on the integration of computational tools and ML techniques that are transforming the field.

2.1 Transit Method

According to Malik and Jara-Maldonado [21][18], the transition from transit detection to machine learning approaches to aid in exoplanet discovery is a major shift in astronomy research. The ML techniques offer new choices to supplement travel strategies, delivering more exact discovery results and greater capacity to identify. Transit strategies assumed a pivotal part in missions, for example, Kepler and TESS which collected monstrous information; Malik et al gave extra proof. The team led by Jara-Maldonado developed a method for successfully searching for planets that have endured the test of time. The library utilizes highlights of TSFresh to direct research as well as training to gather subtleties from light bends as well as inclination supporting classifiers for both practice and examination setting. Furthermore, these devices were utilized to remove highlights utilizing light bends and as slope supporting classifiers. Jara-Maldonado offers an outline of various AI (ML) strategies, for example, profound learning and multiresolution examination which have encountered critical progressions in the field starting around 2011. Her show exhibits how progressions in software engineering have extraordinarily worked on the exactness and viability of searching for exoaplanets. Random Forest Classifiers (RFCs) and Convolutional Neural networks (CNNs) Two computer-aided learning (ML) methods used for Exoplanet Detection, have proven great promise as techniques. Jones et al. [12] released two of these approaches that have highlighted the successes. RFC has efficient ways of handling large-scale transit survey data with high accuracy, and includes priority and feature filtering that ensure accurate detection of signals from exoplanets and reduce false positives. Smith and his colleagues [12] have shown the power of CNN to analyze light curve data. the ability of CNN to process huge quantities of information that resembles images was vital in understanding differences in the brightness of stars that indicate the transit of exoplanets. In the end, these ML methods represent a significant advance in the study and detection of exoplanets to gain more insights on distant worlds.

Chintarungruangchai as well as Jiang have created and evaluated a two-dimensional convolutional neural network (2D-CNN) method for the detection of exoplanet-exoplanet transits using light curves of Kepler Data Release 25 as input data [16]. The researchers conducted extensive tests with various deep learning models with special attention of using 2D-CNN with phase folding to provide an advanced enhancement of transit signals method when the folding times are different from transit time. This study explored various areas of AI and machine learning including logistic regression as well as feature extraction, and the effect of signal-to-noise ratios on the performance of models. Researchers investigated what transit phases affected the accuracy of detection. CNN models that fold proved to have excellent accuracy despite change in transit phases, offering an impressive proof of deep-learning techniques that are applied to data from exoplanets for detection of exoplanets. This study is both an accomplishment and proof of concept as Exoplanet Discovery Tools. Astro ImageJ was widely utilized in Lydia Shannon and colleagues' research project called Exoplanet Transits: Light Curve Photometry [3]. Their research paper demonstrates its utility. ImageJ's version for Astro was essential for creating exact light curves for target images and Astroimagej photometry software helped in identifying and analyzing targets as well as comparator stars easier and facilitated the extraction of vital data from the stars. Astro ImageJ was a key element of this project's accomplishment by providing an advanced method of analyzing light curves using geocentric Julian dates for the index and the stars of the comparator as its y-axes. Astroimagej ability to create light curves provided researchers with valuable information about characteristics of exoplanets, such as the dimensions, transit times and orbital properties which they were studying in this research project.

2.2 Radial Velocity Method

One of the primary methods which have dominated exoplanet detection: the radial velocity (RV) method, measuring the wobble of a star caused by an orbiting planet. While powerful, each method has limitations. RV is impactful at detecting massive planets close to their star, but struggles with smaller, distant ones. There are some techniques or packages that are being used to do the exoplanet detection. The paper "RadVel: The Radial Velocity Modeling Toolkit" by Benjamin J. Fulton and others did a study that focuses on RadVel, an open-source Python package for modeling Keplerian orbits in radial velocity (RV) time series data. RadVel is designed to assist in the detection and characterization of exoplanets using the radial velocity method.RadVel's design is detailed, including its parameterization and Bayesian inference approach [7]. This underpins the software's ability to effectively model and interpret radial velocity data.Although it needs to update and enhance

RadVel's capabilities, suggesting areas like Gaussian Process noise modeling to be incorporated [7].

In the search for exoplanets, using radial velocity, another technique which is the precise radial velocity (PRV) method, has a good potential.It helps obtaining bulk density and thereby understanding the structure and composition of transiting exoplanets [10]. But this needs to be more improved in future because of the need for more photons (larger telescopes), more stable spectrographs, better calibration, and improved correction for stellar jitter to push towards the detection of Earth-like exoplanets. It also calls for long-term commitment and investment in PRV surveys and technology development [10]. PRV is a powerful method for detecting exoplanets, particularly when used in addition with other methods like transit photometry, enabling a more good understanding of exoplanetary systems.

2.3 Direct Imaging Method

Using machine learning to find exoplanets is a major departure from existing techniques. The results of several studies are compiled in this review to show how effective they are as tools for astronomical research.

Direct imaging techniques have proven to be one of the most useful in locating exoplanets that are brighter than the host stars [4]. When locating exoplanets using this method, the primary selection criteria are spatial separation and brightness ratio. It performed better than other approaches. Direct imaging has garnered a great deal of praise from the scientific community for its reliable mapping and analysis of exoplanetary elements.

Deep learning is a crucial strategy when it is combined with direct imaging to address exoplanet detection issues like weak signals or insufficient data for supervised learning [20]. In order to train CNN to locate planets in direct imaging data, researchers have created synthetic datasets using GAN. Deep learning has greatly improved the detection of faint signals, which is difficult for traditional methods. This study shows how the use of CAM (class activation maps) to target exoplanet discovery through machine learning has transformed direct imaging.

On the other hand, identification of exoplanets is challenging in high contrast environments. But it has advanced substantially. One significant tool has been the clever fusion of statistics and deep learning known as PACO.In this framework, specialists have gotten PACO's reliable contraptions nearby the latest levels of progress in huge learning [29]. This procedures with how we could unravel objects in space past our enormous structure by unequivocally finding exceptional bodies. With this one's receptiveness, the assessment of far off magnificent bodies in space has advanced further.
Like this, one evaluation of the revelation of exoplanets used joining high-offset imaging with reiterated data to consolidate the information. This technique was effective for measuring high-balance pictures with express datasets and worked with issues like spot models and feeble signs [9]. The tremendous impacts that human information has had on the investigation of cosmology, especially on the assessment

and receptivity of exoplanets, should be visible in this framework. This ability is changing our perception of the world and the manner in which we research distant excellent articles.

Moreover, CNN alongside the specialized Starshade imaging technology can be used to search for exoplanets. But in such cases, problems like weak signals and complex patterns may arise. But to tackle such problems in exoplanet images we employ a new CNN architecture called U-Net. Some researchers trained these CNNs on a synthetic dataset and found that they outperformed conventional methods and suggested that CNNs could transform the way we analyze exoplanet images[28]. The usefulness of CNNs for this kind of research was also discussed in the paper ”Exoplanet Detection from Starshade Images Using Convolutional Neural Networks.”

Our methods for finding exoplanets have improved as a result of these studies. These researchers have increased the effectiveness and precision of the search for far-off celestial objects. It helped us advance our understanding of astrophysics by combining deep learning techniques and direct imaging. As we discover more exoplanets to study, combining traditional astronomy with computational technologies will open up new and exciting avenues for universe exploration.

2.4 Astrometric Method

Astronomic Approach primarily focuses on the integration of Machine Learning (ML) algorithms and big data tools in astronomical research, particularly in astrometry for detecting extrasolar planets. The significant advancement in astronomical data size and complexity necessitates the development of data-driven science. Machine learning algorithms have become increasingly popular among astronomers for a variety of tasks due to the rapid growth in data volume and complexity in astronomy [15]

Astrometry, the precise measurement of a star's position in the sky, is crucial for detecting the gravitational influence of orbiting planets. The shift from ground-based telescopes, limited by atmospheric interference, to sophisticated space missions like ESA's Gaia has been monumental. Thousands of gas giant planets have been discover by Gaia's mission, with its capacity for highly precise measurements [6]

In the documents we chan see that there are various aspects of astronomical detection, which includes the types of data required, the methodologies for extracting and modeling the planetary signals, and significance of detections. It highlights the application of both monopupil and diluted-aperture telescopes and covers all the advanced methods in astrometric analysis applicable to various observational modes [33]

The angular position of a star as measured by instruments, varying from one-dimensional measurements in missions like Hipparcos and Gaia to two coordinates on ground-based telescopes is a mater of concern of The observable model in astrometry. In this model, we can see the optical path-length difference between interferometer arms in instruments like NASA's SIM or the HST FGS. With space-based measurements which offers the freedom from atmospheric turbulence [24], These measurements can be executed in wide-angle or narrow-angle modes

Instrumental, atmospheric, and astrophysical noises are affected by astrometric data. Accurate modeling to eliminate or reduce these noises is very important to enhance the precision of astrometric measurements. Instrumental noise which indicate random photon errors and systematic errors, while atmospheric noise encompasses effects like differential chromatic refraction (DCR) and atmospheric turbulence. Astrophysical noise which arises from the target environment, also significantly affects precision [27].

Applying both observable and noise models to data is involved in The estimation process in astrometry. Search techniques, hypothesis testing, and parameter estimation, often utilizing a generalized least-squares method is include in this process. Aso it includes matching the data with model parameters, accounting for deviations using the noise model. Approaches like Iterative approaches are necessary for dealing with non-linear functional forms in the observable model [8],

It is confirmed by the Ground-based astrometric experiments that the limitations of monopupil telescopes to milliarcsecond precision. Experiments have shown atmospheric precisions and the impact of using dense star fields as reference frames. Long-baseline optical/infrared interferometry experiments have demonstrated more acurate results in terms of wide-angle astrometric precision [31].

Space-based experiments like the HST FGS and the Hipparcos satellite have significantly advanced astrometric measurements. Various calibration and data-reduction procedures have been implemented by them to reduce the error percentage in astrometric reference frames. The probability of finding a suitable reference star for planet searches and the technological goals of space-borne instruments like SIM and Gaia have been discussed, highlighting their aim for high precision in measurements [26]. Because of the exploration of astrometry, detecting exoplanets has evolved significantly, starting from ground-based observations to highly precise space missions. Because the machine learning algorithms and big data tools are introduced to this experiments, we can see the improvement in effectiveness of astrometric observations, enabling astronomers to extract meaningful data and contribute to the understanding of planetary systems beyond our own. Astrometry stands as a testament to human ingenuity and the relentless pursuit of knowledge, continuously evolving and promising new insights about our universe .

2.5 Gravitational Microlensing Method

In the study, Christie demonstrates how gravitational microlensing can be used to detect exoplanets using small (0.35m) telescopes and CCD cameras. By observing high-magnification events that are sensitive to the presence of planets, it emphasizes that even small telescopes can contribute significantly to the detection of exoplanets[1]. One impediment noted in the review is the test of seeing in metropolitan regions with light contamination and frequently overcast circumstances. Notwithstanding, the review defeats these by focusing on projects that can endure interferences and by utilizing a quick information procurement methodology during clear sky periods. The viability of little telescopes in metropolitan settings is likewise featured, as they can rapidly redistribute time to notice fascinating occasions. By and large, the review presents a promising way to deal with exoplanet identification utilizing unobtrusively estimated telescopes, featuring their expected job in growing cosmic examination capacities.

In the study of Tsapras' is used gravitational microlensing for finding the exoplanets.The strategy is compelling in distinguishing planets which are challenging for recognising different methods. Particularly, it is situated a long way to their host stars[13].However, there are some limitations in this paper, such as, interpreting complex light curves and occurrences of microlensing events. To overcome these challenges, they used cutting edge modeling strategies and high caliber observations.

Gravitational microlensing is taken as a method for finding exoplanets in the concentrate by Zakharov, Calchi Novati, De Paolis, and Ingrosso. This system is strong in finding planets that are by and large missed by various philosophies, especially those far from their host stars. At any rate, the examination raises difficulties [2], including the remarkableness of microlensing events and the difficulty in unraveling the ensuing data. The review recommends that to determine these issues, innovative discernment and refined information assessment frameworks that consider the possible results of productive planet affirmation are required. The evaluation remembers the enormous limit of gravitational microlensing for the field of exoplanet receptiveness.

In Cassan's assessment, gravitational microlensing is used to find extrasolar planets. The strategy effectively identifies low mass planets at huge orbital good ways from their stars. In any case, the flightiness of microlensing occasions and the bizarreness of information translation present inconveniences[5]. Cassan features the crushing essential for reliable checking and obvious level assessment structures to decide these issues to legitimately see and handle exoplanets utilizing microlensing and in this manner contribute by and large to the field.

Gaudi et al.'s research is looking into the possibility of finding exoplanets using gravitational microlensing. This system is shown to areas of strength for particularly seeing planets that are overall around difficult to see, especially those at critical uncommon ways from their host stars [14]. The hardships accomplished by the momentousness of microlensing occasions and the trouble of information translation are the mark of combination of the appraisal. To overcome these impediments and basically work on our ability to translate exoplanetary plans, Gaudi and his accomplices stress the significance of developing new pieces of information and complex evaluation procedures.

In this research, we investigate several established techniques for detecting exoplanets, including the Transit Method, Radial Velocity Method, Direct Imaging, Astrometry and Gravitational Microlensing and identify an optimal choice. These approaches played, and continue to play, a central role in driving exoplanetary science, but each has its strengths and its weaknesses. Large, close-orbiting exoplanets have been found by the Transit and Radial Velocity methods, but only large and close exoplanets. Astrometry and Gravitational Microlensing have degrees of freedom to access exoplanets in distant orbits; however they are limited with complex data interpretation and signal to noise.

On the other hand, the Direct Imaging way provides a more flexible approach which enables exoplanets to be directly imaged and provides complete information on exoplanets' atmospheres, sizes and orbital parameters. However, with recent improvements in machine learning particularly Contrastive Learning, it has become possible to overcome the issue of faint signal detection, so that Direct Imaging becomes possible again. Where sublte features in complex datasets need to be contrasted, Contrastive Learning effectively distinguishes such features to allow for more accurate detection and classification of planets around other stars, specifically in high contrast environments where the signal is weak relative to the stellar noise.

This research takes advantage of Contrastive Learning within the structure of Direct Imaging in an effort to overcome inherent limitations of all current and new detection methods. By refining exoplanet identification through the improvement of the model's learning of differences in image data, the approach can enhance the ability to identify faint exoplanets. Consequently, this combined method not only tackles the difficulties of high contrast imaging environments, but also provides new avenues to explore exoplanetary systems which were previously hard to observe.By integrating Direct Imaging with Contrastive Learning, a more detailed and precise analysis of distant planetary systems is made possible. This approach could help deepen our understanding of exoplanetary environments and the overall hunt for habitable worlds in the galactic neighborhood.

Chapter 3

Methodology

The initial step in our methodology involved compiling a dataset of JWST MIRI coronagraphic images. Given the nature of these space images, preprocessing was essential. We began by normalizing the images, converting them from PNG format to FITS. To handle missing pixels, we applied median filtering and Navier-Stokes inpainting techniques. Additionally, we enhanced image contrast and applied super-resolution methods to improve resolution. The dataset was then split into two subsets: training (80%) and validation (20%). Augmentation was performed exclusively on the training set, which involved rotating, flipping, and scaling the images. Following preprocessing, the augmented images were input into our custom model. The first component of the model is the enhanced contrastive exoplanet detection module. The backbone layer of this module utilizes ResNet-18, which extracts high-dimensional features (512 dimensions) from the images. These features are subsequently passed to the embedding layer, where dimensionality is reduced to 16, retaining only the most salient features. The model includes two classifier layers: one for stars and one for exoplanets, both of which yield binary outputs indicating the presence or absence of the respective celestial bodies. Few-shot learning is integrated with the embedding layer, enabling the model to efficiently learn from a limited number of labeled examples, thereby improving feature extraction and classification performance, especially in cases with scarce labeled data. The model was trained over 25 epochs, with early stopping implemented to prevent unnecessary computation once the performance plateaued. Additionally, dropout layers were integrated within the architecture to reduce overfitting, ensuring robust generalization to new data.

After classification, the images are stored in a list and subsequently passed to YOLOv5 and then YOLOv7, with localization results from each model compared to determine optimal performance in identifying the precise locations of stars and exoplanets in each image. This comprehensive approach leverages contrastive learning, few-shot learning, and advanced classification and localization techniques to detect and accurately localize exoplanets and stars from JWST MIRI coronagraphic observations.Figure 3.1 shows the overview of the proposed exoplanet and star detection system.

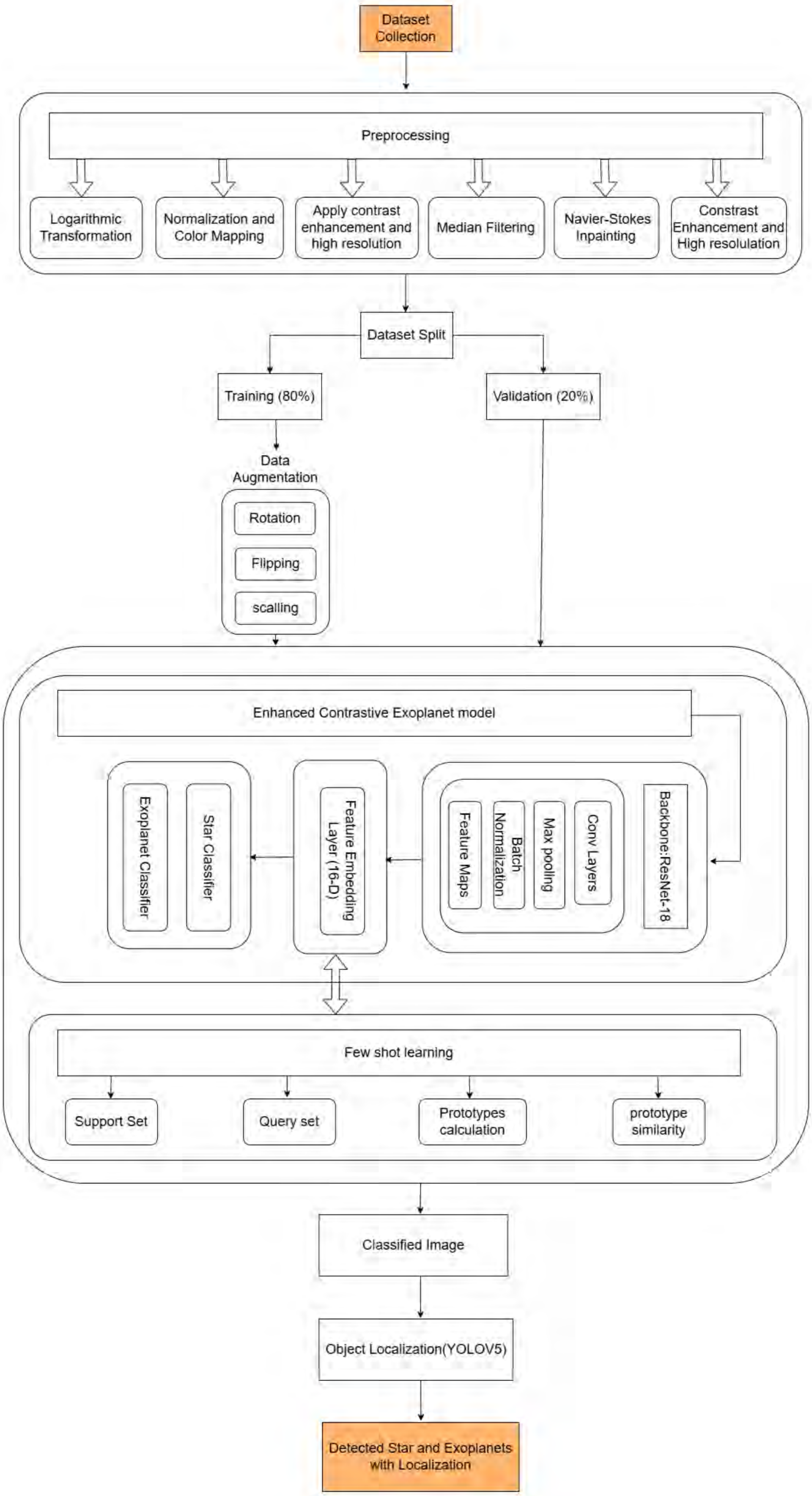

Figure 3.1: An Overview of the Proposed Exoplanet and Star detection system Leveraging Contrastive and Few Shot Learning

3.1 Dataset Collection

The dataset in this study includes high-resolution direct imaging observations using JWST from the sample with the MIRI in the coronagraphic imaging mode . To enhance visibility of the adjacent exoplanetary bodies to the place near their stars, observations were made using the filters F2300C and LYOT_2300 to select precise IR bandwidths. Data acquisition was programmed to level 3 image processing to yield the best results for scientific application. The data to create the images included in this paper were obtained from the Mikulski Archive for Space Telescopes (MAST) and the ESA JWST Archive [37] [36]. These resources enabled accurate flagging according to mission parameters, specifically JWST, and instrument settings, MIRI/coronagraph. Furthermore, direct imaging exoplanet candidates in the dataset were cross checked and validated using the physical archive known as NASA Exoplanet Archive. By searching only in the coronagraphic images, the sample was simply and effectively purged to remove all contaminated light from the star that could potentially mask any planetary object that may be present.

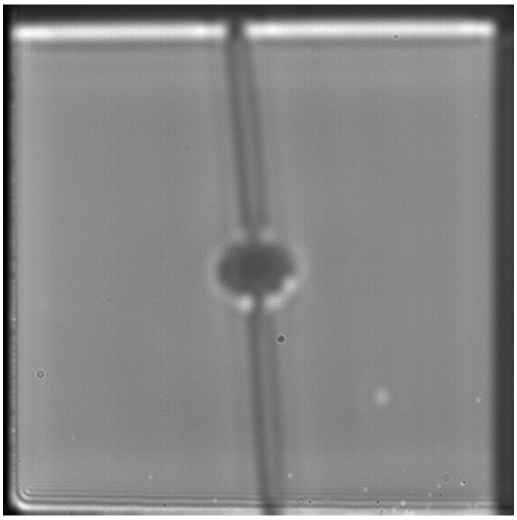

Figure 3.2: Exoplanet with Star

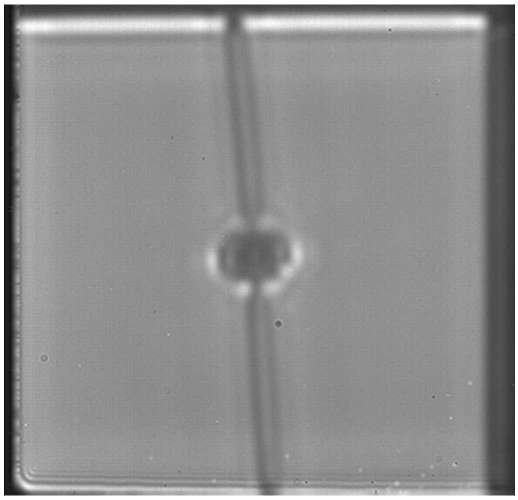

Figure 3.3: Only Star

Each image in the dataset, such as those shown in Figures 3.2 and 3.3, represents typical coronagraphic imaging results. In Figure 3.2, we see an exoplanet orbiting its host star. The bright central feature corresponds to the star, which is blocked using the coronagraphic technique to reduce its overwhelming brightness, allowing a clearer view of the nearby exoplanet. The faint object seen near the central star is a potential exoplanetary candidate, whose detection is made possible by this technique.In contrast, Figure 3.3 shows an image where only the host star is present without any visible exoplanets. The coronagraph blocks the central star's light, but since no dim objects are visible around the star, this image represents a stellar system without detectable exoplanets.

Each image in the dataset was sampled at a high resolution, providing clear spectral data for subsequent analysis. The chronographic imaging technique allowed the dataset to capture objects with varying brightness levels, from the intense light of the stars to the faint signatures of orbiting exoplanets. Images were saved in multiple formats, including FITS and PNG, to ensure compatibility with the processing pipeline and machine learning models used in this study.The key characteristics of the dataset are summarized in Table 3.1:

Table 3.1: Dataset characteristics for exoplanet direct imaging.

Hallmark	**Volume/Details**
No. of observations	3114 observations
Instrument	JWST (James Webb Space Telescope)
Filters	F2300C, LYOT_2300
Observation mode	Coronagraphic Imaging
Product type	Processed images (Level 3)
Recorded data type	Direct imaging
Imaging resolution	High-resolution
Data sources	MAST Portal, ESA JWST Archive, NASA Exoplanet Archive
No. of labeled exoplanets	1866 confirmed exoplanets
Total processed images	3114 processed images
Train images	2502 images
Validation images	612 images

3.2 Data Pre-Processing

3.2.1 RAW FITS file Pre-Processing through AstroImageJ

The first step of our image processing workflow involved pre-processing the RAW FITS files using AstroImageJ (AIJ) [34], a widely used tool in astronomical data analysis. Due to the inherent challenges of direct imaging such as the faint nature of exoplanets in proximity to bright stars many of the acquired images were too dark to discern important features. To this end, the images presented were processed with AIJ [34], which operates with brightness and contrast enhancing algorithms making these improvements while not distorting the scientific content of the data set. The brightness and contrast functions of AstroImageJ [34] were useful for enhancing the variability between the compact and diffused regions for the purpose of highlighting the weak brightness from the exoplanets. In this process, it became easier to ensure that the desirable attributes in the images were more apparent, especially when using advanced detection models in subsequent data analysis. Apart from simple brightness and contrast controls, which turned out to be to important for stretching the fainter data to better compare them to the brighter data, AIJ offered other essential functionalities for data calibration and metadata management. To perform the bias, dark and flat-field corrections we used the integrated features of the system. Moreover, using the functionalities of AIJ we were able to integrate with Astrometry.net for plate solving and we included WCS to the images thus the accurate spatial reference of naked eye stars as well as exoplanets was achieved. This preparation was very important for ensuring the reliability and efficiency of the following analytical processes.

3.2.2 Converting dataset from FITS format to PNG format

We converted the astronomical imaging data from the Flexible Image Transport System (FITS) format into Portable Network Graphics (PNG) format for easy manipulation and visualization in our work. We loaded in the files using the Python scientific libraries: Astropy for reading FITS files and Matplotlib for saving images in PNG format. The FITS files were loaded, and we extracted the image data. The resulted data was treated and normalized in order to improve visual clarity. The processed images were saved in PNG format to further their analysis and visualization. This conversion process was applied to all FITS files in the dataset to maintain consistency and to help machine learning tasks and other analysis workflows process FITS files more easily.

3.2.3 Pre-process using Median Filtering and Navier-Stokes Inpainting to Detect and Fill Missing Pixels

In our study, one of the main preprocessing consisted in detecting and fill missing pixels in the dataset images. Incomplete data, arising from missing pixels, can have a negative effect in subsequent analysis, especially if working with high resolution astronomical imagery. To address this, we employed a two-step method: To observe how to first detect missing pixels using a mask generation technique, and then fill them using a combination of median filtering and inpainting.
A mask was generated to detect missing pixels. The grayscale images were assumed to be missing pixels with a value of zero, and these were marked in the mask by identifying the pixels where these would occur in them. Utilizing morphological operations of dilation and erosion, the mask was refined further to ensure correct capture of the missing areas.
After identifying the missing pixels, the next step was filling these gaps using two techniques:

- **Median Filtering**:In the smoother regions the missing pixels were filled via median blur technique. The missing pixel values are then replaced with the median value of surrounding pixels which facilitates the natural texture of the image.
- **Navier-Stokes Inpainting**:The Navier Stokes inpainting method was applied on higher level of detail in more complicated regions corresponding to the provided structure. The inpainted pixels are reconstructed using the surrounding pixel values and iteratively, portions of the image are filled, so the areas inpainted blend well with the rest of the image.

In addition, there was bicubic interpolation of the images to higher resolutions which improved clarity and resolution of the final output. Once inpainted and resized, the images were stored as PNG format for further analysis.

3.2.4 Pre-process using Contrast Enhancement and High Resolution

In addition to filling missing pixels, another crucial preprocessing step in this study involved enhancing the contrast of the images and increasing their resolution. These techniques were applied to ensure that important features, particularly faint exoplanetary signals, could be clearly distinguished from the background noise.

Specifically, faint exoplanets in direct imaging necessitated enhancement of the contrast in order to enhance visibility of subtle features. This increased the difference between bright and dark regions, and helped to read out the exoplanetary signals next to the bright stars. A histogram equalization technique was used to adjust image intensities to make the histogram distribution more uniform and contrast enhance [38] . This improved visibility of low intensity regions that are critical in detecting faint objects.

In this study, we also boost image resolution to aid more detailed analysis. Bicubic interpolation was utilised to upscale. This technique is bound to use pixel values that smoothly transition from one value to the next, and thereby reduces the chances of putting noise or artificats during resizing. When trying to detect tiny and faint exoplanets near bright stars, increased resolution is very important, and we were able to get better resolution than previous observations enabled us to.

The combination of contrast enhancement and high resolution upscaling together improved the overall quality of the dataset so that important features were preserved and enhanced for these subsequent machine learning based detection and classification tasks.

3.2.5 Data Annotation

In this study, the dataset was carefully labeled to distinguish between two primary classes: stars and exoplanets. As such, the labeling of each image was performed manually in the **CVAT** [35] annotation tool, and each image was labeled for either the presence of a star or exoplanet, or both. The dataset was divided into three sets: training, validation and testing. The labels were assigned in two categories for the dataset. Each set is contained with images with annotated bounding boxes around stars and exoplanets, thus, allowing precise labels for the object detection tasks. These images have labels "0" when only the stars can be seen, and "1" when an exoplanet can be seen near the star. Each member of our group individually examined and annotated the images for the presence of exoplanets and stars. After completing individual annotations, we compared and analyzed our results collectively. For each image, we employed a majority voting system to finalize the label, determining whether an image contained an exoplanet, a star, or both. Based on this consensus approach, we ensured consistent and accurate labeling across the dataset, resolving any ambiguities by leveraging group agreement. The clear classification of celestial objects supplied by this binary labeling system was crucial for training the machine learning model.

The model was consistently learning to differentiate the two classes with labeled data applied consistently on all sets, so that it should be able to perform correctly while in training, and validation and test. Using the structured labeling approach, the dataset was prepared for the object detection tasks enabling the identification of faint exoplanets alongside bright stars in high resolution astronomical images. On the other hand, our five-member team completed the augmentation together. After finishing, we voted on the corrected augmentations for stars and exoplanets, and chose the final options based on majority agreement.

3.3 Dataset Split

For the purpose of this study, the dataset was divided into two distinct sets:

3.3.1 Training Set

This subset consisted of 2502 processed images, each labeled based on previous scientific observations of exoplanetary candidates. Among these, 1866 images contained both exoplanets and their host stars, while the remaining images featured stars without accompanying exoplanets.

3.3.2 Validation Set

This subset contained 612 number of images used for hyperparameter tuning and model validation. These images helped optimize the model without being exposed during training, ensuring that the model generalized well to unseen data.

3.4 Feature Extraction

In this work, we demonstrate that feature extraction is a crucial part of the exoplanet detection pipeline, where the objective is to efficiently transform input images into meaningful representations that can be classified. In this work, we use a pre trained ResNet18 model as the backbone to extract high level feature from astronomical images. Extracted features are then transformed to a lower dimensional embedding and used as input for the classification layers used to separate stars from exoplanets.

3.4.1 ResNet18 Backbone

ResNet18 is a neural network with 18 layers that effectively identifies patterns and features in images. Its deep architecture and residual connections mitigate issues such as vanishing gradients, allowing for accurate training across multiple layers [32]. These connections facilitate the transfer of features, making ResNet18 particularly useful for complex data.

- **Pre-trained Model:** ResNet18 was trained on ImageNet, which consists of over a million images [32]. This extensive pretraining enables the model to recognize broad features, including edges, textures, and shapes. Such capabilities are beneficial in fields with limited labeled data, such as exoplanet detection, as the model can generalize from common features. Consequently, this reduces the dependency on a large labeled dataset for detecting exoplanets.

- **Fully Connected Layer Removal:**To customize the model for specific tasks, such as analyzing astronomical data, the final fully connected layer of ResNet18 is removed after pretraining. This alteration allows the model to output a 512-dimensional feature vector, which effectively represents the input image without the constraints of the original classification head[32].

- **Output of the Last Convolutional Layer:**The output from the last convolutional layer is a 512-dimensional vector that serves as a condensed and informative representation of the input image [32]. This vector incorporates both low-level features, like edges and textures, and high-level features, such as shapes and structures.

- **Feature Vector:**The 512-dimensional feature vector is well-suited for tasks like embedding and classifying images[32]. In the context of exoplanet detection, this feature vector captures the essential details required to distinguish stars from potential exoplanets, especially in noisy images.

3.4.2 Embedding Layer

In order to reduce computational complexity and increase performance of the model, a ResNet18 backbone backbone is followed by a fully connected embedding layer. This layer compressed 512 dimensional feature vector output from ResNet18 to 16 dimensional using small vector IMb can reduce the dimensionality of the 512 dimensional feature vector output from ResNet18 to 16 dimensional embedding. However, this dimensionality reduction is a necessity for efficient classification and few shot learning tasks.

- **Dimensionality Reduction:** The features from the input high dimension space are projected to a 16 dimensional space by embedding layer, reducing computation and unnecessary or redundant information. Furthermore, the reduced dimensionality allows distances between embeddings to be computed more simply, a key component of most few-shot learning frameworks such as Siamese Networks.

- **Learnable Embeddings:** The embedding layer is made with learnable parameters and the model picks them up and tries to learn during training. As a result, the model can generate the most informative and distinguishable embeddings for different image types, which aids in the effective classification of stars and exoplanets.

- **Shared Embedding Space:** Both the star and exoplanet classifiers utilize the same 128-dimensional embedding space. This shared space enables the model to learn general features relevant to both classes while also focusing on specific patterns for distinguishing between stars and exoplanets.

3.4.3 Contrastive Learning for Better Embeddings

Supervised learning is also combined with contrastive learning to extract the feature embedding, so that the embeddings are well clustered and separable. Contrastive learning [17] encourages the network to bring similar images closer in the embedding space while pushing dissimilar images farther apart. This approach enhances the quality of the learned embeddings, making the model more robust in scenarios with limited or noisy data.

- **Positive and Negative Pairs:**During training, pairs of images are generated, with positive ones consisting of images taken from the same object (e.g. two images of stars) and negative ones containing images of different categories (e.g. one image of a star, and one image of an exoplanet). Distance between positive pairs and negative pairs in the embedding space is minimized and that between negative pairs are maximized [17].

- **Contrastive Loss Function:**In order to train the model on meaningful embeddings, we use a contrastive loss function. The model is trained to group images of the same class and separate those of the different classes, by this loss function. This leads to improving classical classification accuracy as well as few shot learning performance.

3.4.4 Role of Embeddings in Few-shot Learning

In the context of few-shot learning [11], where the model must classify new images with limited labeled data, the quality of the 16-dimensional embeddings becomes critical. Few-shot learning methods, such as Siamese Networks, rely on the ability to compute mean embeddings for each class, known as prototypes. The model's ability to correctly classify unseen images depends on how well it can compute distances between the embeddings of new images and these class prototypes.

- **Embedding Space for Siamese Networks:** By reducing the dimensionality from 512 to 16, the embedding layer simplifies the task of computing distances between class prototypes and query images. This dimensionality reduction is especially beneficial in few-shot learning settings, where only a small number of labeled examples are available, but accurate predictions are still required.

This feature extraction pipeline, combining the ResNet18 backbone with contrastive learning and embedding-based dimensionality reduction, provides a robust foundation for exoplanet detection. The system not only reduces computational complexity but also enhances classification performance, particularly in challenging few-shot learning scenarios.

3.4.5 Visualization of Feature Embeddings Using t-SNE

To better understand how well the model distinguishes between stars and exoplanets, we employed t-distributed Stochastic Neighbor Embedding (t-SNE) [22], a nonlinear dimensionality reduction technique, to project the high-dimensional embeddings into a 2D space. The t-SNE plot 3.4 illustrates the separation between stars (label 0) and exoplanets (label 1), with distinct clusters for each class. This visualization highlights the model's ability to generate discriminative features, reinforcing the effectiveness of the feature extraction process [22].

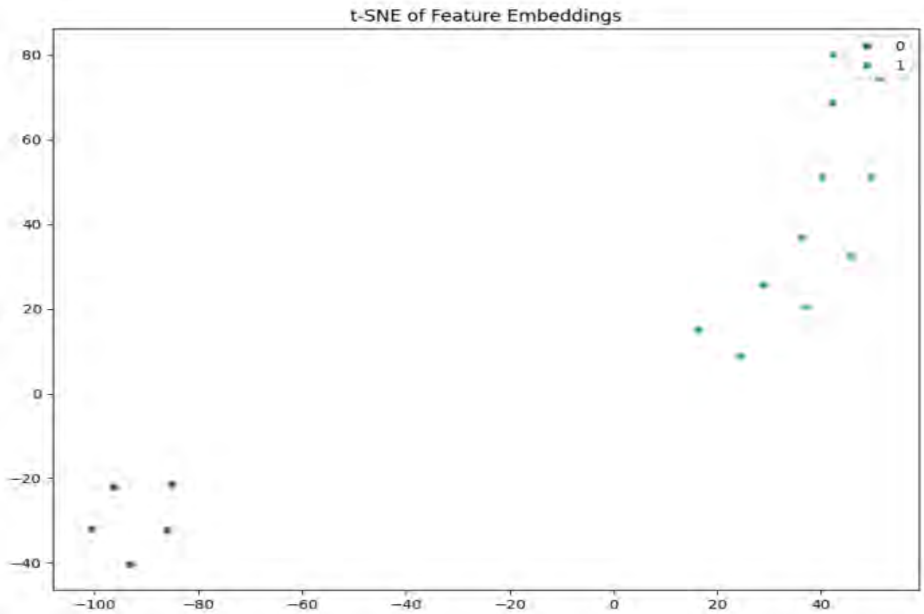

Figure 3.4: t-SNE visualization of embeddings, showing distinct clusters for stars and exoplanets.

3.4.6 Visualization of Convolutional Feature Maps

In addition to embedding visualization, we also explored the intermediate feature maps produced by the convolutional layers of the model. Figure 3.5 shows the feature maps extracted from a deep convolutional layer when applied to input images. These maps capture various levels of abstraction, ranging from low-level textures and edges to high-level structures associated with stars and exoplanets. The feature maps demonstrate the model's capacity to extract detailed and meaningful representations, which are crucial for distinguishing subtle differences in astronomical images.

Figure 3.5: Visualization of convolutional feature maps from deeper layers of the model.

3.5 Contrastive learning based classification model

Contrastive learning is a self-supervision learning method focused on learning samples' similarities and differences between two samples by projecting them onto a low-dimensional space. Self-supervision: the model creates its own labels or tasks out of the data, so, it is able to learn useful representations without reference labels [19]. This is done by obtaining pairs or groups of samples describing positive samples, or different groups describing negative samples based on data augmentations, or contextual information.Figure 3.6 shows our model architecture.

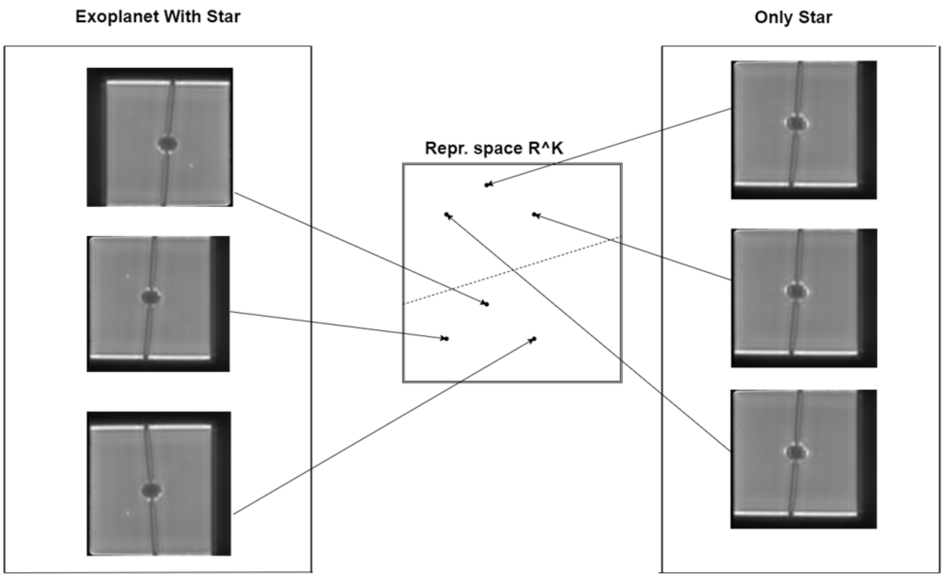

Figure 3.6: Contrastive learning Architecture

The core idea of contrastive learning is to make the embeddings of similar samples (positive pairs) closer in the embedding space, while pushing apart the embeddings of dissimilar samples (negative pairs) [19].This approach is most effective when there is sparse labeled data, because it uses the inherent structure in this data to train for the feature representations. While contrastive learning learns an embedding space by using augmentations or predefined structures in the data, subtle but crucial patterns are learned.The contrastive loss defined in eqn [1]:

$$L_{contrastive} = (1-y)\frac{1}{2}(D^2) + y\frac{1}{2}(\max(0, m-D))^2 \tag{1}$$

Where:

- y is a binary label indicating pair similarity, where $y = 1$ for similar pairs and $y = 0$ for dissimilar pairs,
- D represents the Euclidean distance between the embeddings of the paired samples,
- m is a margin parameter that ensures dissimilar pairs are separated by at least this distance in the embedding space.

The Enhanced Contrastive Exoplanet Model(ECEM) identifies, depending on the result of the classification, whether the input image contains a star, an exoplanet, or both. After extracting meaningful features from the input images using the ResNet18 backbone and embedding layer, these features are passed to two separate classifiers: So, one was to detect stars for which one glance was enough, and another was to detect exoplanets. We aim at predicting binary labels for each image: One sign that looks like a star and one sign that looks like an exoplanet. Classification process is described in ECEM Invention to distinguish whether an input picture contains or lacks a star, an exoplanet or both. After extracting meaningful features from the input images using the ResNet18 backbone and embedding layer, these features are passed to two separate classifiers: This one is for finding the stars, and this other one is for finding the exoplanets. To classify the image, we want two label outputs of whether there is a star or exoplanet in the image.

3.5.1 Star and Exoplanet Classifiers

Over two independent classification layers, we construct two classifiers over a shared 16 dimensional embedding layer. The rich information encoded in the feature embeddings are leveraged by these classifiers by using simple but effective architectures to perform binary predictions for all tasks.

Separate Classifiers for Star and Exoplanet Detection

Each classifier is designed to handle a binary classification problem, where the output is a single value: 0 or 1. The **star classifier** predicts whether a star is present in the input image, while the **exoplanet classifier** predicts the presence of an exoplanet. The overall architecture of each classifier is described below.

Linear Layers

The classification task begins by passing the 16-dimensional embedding output from the feature extraction process into a series of fully connected (linear) layers. These layers map the embedding vector into a smaller space, progressively refining the feature representation for the final prediction. Each classifier follows this structure:

1. **First Linear Layer**: The 16-dimensional embedding is fed into a fully connected layer that projects it into a lower-dimensional space, typically smaller than 16 dimensions. This dimensionality reduction helps focus the model's attention on the most critical features for classification.

2. **ReLU Activation Function**: After the first linear layer, a **ReLU (Rectified Linear Unit)** activation function is applied to introduce non-linearity into the model. The ReLU function is defined in eqn [2] which introduce non-linearity into the model.

   $$f(x) = \max(0, x) \tag{2}$$

   This ensures that the classifier can learn complex decision boundaries, essential for distinguishing between the presence or absence of stars and exoplanets.

The ReLU activation ensures that only positive values pass through, filtering out less important or negative feature values.

Final Linear Layer and Sigmoid Activation

After the first linear layer and ReLU activation, the refined features are passed through another fully connected layer. This layer outputs a single scalar value representing the model's confidence in the presence of the object (star or exoplanet).

3. **Sigmoid Activation Function**: To convert this raw output into a probability, a **sigmoid activation function** in 3 is applied. The sigmoid function squashes the output into a range between 0 and 1, making it interpretable as a probability value. The sigmoid activation is defined in eqn [3]:

$$\sigma(x) = \frac{1}{1 + e^{-x}} \tag{3}$$

The sigmoid function ensures that the output can be interpreted as a probability, where values closer to 1 indicate a higher likelihood of the presence of a star or exoplanet, while values closer to 0 indicate their absence.

Binary Output and Thresholding

The final prediction for each classifier is obtained by thresholding the sigmoid output. Specifically:

- If the sigmoid output is greater than or equal to 0.5, the model predicts that the object (star or exoplanet) is present (i.e., output = 1).
- If the sigmoid output is less than 0.5, the model predicts that the object is not present (i.e., output = 0).

Final Output

In summary, the **star classifier** outputs a binary prediction of 0 or 1 for the presence of a star, while the **exoplanet classifier** does the same for the presence of an exoplanet. These two binary predictions are combined to form the final output of the model for each image.

3.5.2 Joint Training of Classifiers

Though the star and exoplanet classifiers are meant to be used independently, they are both trained on the same dataset together in order to allow the model to learn to recognize stars and exoplanets in a single step. This joint training approach offers several advantages:

Shared Feature Space

The same 16 dimensional feature embedding is used by both classifiers: the feature embedding is obtained through the ResNet18 backbone and an embedding layer. This shared feature space allows the features learned to be useful across the two related tasks of star detection and exoplanet detection from relative parallax measurements, leading to improved generalization across these two tasks. By sharing this feature space, we achieve efficiency of resource use, since the model learns about meaningful features that separate both astronomical objects.

Efficiency in Learning

By training the classifiers in joint space, training efficiency is achieved, since both classifiers can be trained with the data available. Detecting exoplanets sometimes requires similar detection tools, such as brightness or specific light patterns, and features helpful for star detection (e.g., brightness) might also be useful in detecting exoplanets. The model uses such overlapping features to enhance its performance across both tasks if we train both classifiers on the same dataset.
The process of joint training encourages multi task learning, a process useful with limited labeled data. The model sidesteps one overfitted task to produce shared representations that allow it to become more robust to both stars and exoplanet detection.

3.5.3 Few-shot Learning and Siamese Networks

In scenarios with limited data availability, few-shot learning is critical for tasks like detecting exoplanets. This learning approach allows models to generalize from only a few labeled examples, which is especially useful in exoplanet detection due to the scarcity of exoplanet images [25]. Our model leverages Siamese Networks, a popular few-shot learning technique that determines similarity between pairs of examples rather than relying solely on class prototypes.
Siamese Networks are structured to perform **N-way, K-shot classification** by learning to differentiate between pairs of images. Here, **N** refers to the number of classes, and **K** represents the support examples per class that are used to form pairs for comparison. The network computes embeddings for each image in a pair, and a similarity measure—often based on distance or cosine similarity—determines if the images belong to the same class. For each query image, the model classifies it by comparing it to support images, enhancing its capacity to recognize classes with only a few labeled instances. This approach is particularly suitable for scenarios where defining prototypes is challenging, as it instead relies on pairwise similarity to perform classification.Figure 3.7 shows the architecture of Siamese Network.

Siamese Network Architecture

The architecture of the Siamese Network comprises three main components:

Embedding Extraction The model first extracts embeddings for both the support and query images using a shared ResNet18-based feature extractor. These embeddings, which are 16-dimensional vectors, capture the essential characteristics of each image.

Similarity Calculation For each pair of images, the model computes the Euclidean distance between their embeddings to determine similarity. Given two im-

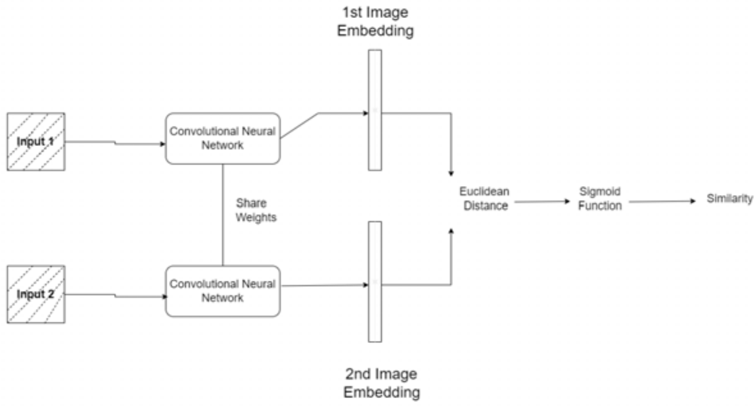

Figure 3.7: Siamese Network Architecture

ages x_1 and x_2 with embeddings $\mathbf{f}(x_1)$ and $\mathbf{f}(x_2)$, the Euclidean distance $d(\mathbf{f}(x_1), \mathbf{f}(x_2))$ is calculated eqn [4] as:

$$d(\mathbf{f}(x_1), \mathbf{f}(x_2)) = \|\mathbf{f}(x_1) - \mathbf{f}(x_2)\|_2 \tag{4}$$

The lower the distance, the more similar the images are considered to be, as judged by the model.

Distance-based Classification For each query image, the model calculates the distance to each support image embedding. The query image is assigned the label of the support image with the smallest distance. The predicted label $\hat{y}_q$ for the query image x_q is given eqn [5] by:

$$\hat{y}_q = \arg \min_{y_i \in Y_{\text{support}}} d(\mathbf{f}(x_q), \mathbf{f}(x_i)) \tag{5}$$

This classification approach leverages the concept that images from the same class will have embeddings closer to one another in the embedding space.

Support and Query Data Processing

The Siamese Network processes support and query data by pairing query images with support images and measuring similarity to classify the query. Key steps for handling support and query data include:

Support Data Processing Support images from each class are sampled from the dataset and pre-processed (resized, normalized, and converted into tensors). These images are passed through the ResNet18 backbone to generate 16-dimensional embeddings used for similarity comparison with query images.

Query Data Processing Query images are similarly pre-processed and passed through the shared network to obtain embeddings. These query embeddings are then compared to the support embeddings using the Euclidean distance metric, allowing the network to assign a label based on the most similar support image.

Few-shot Classification Tasks

To evaluate the model's ability to perform few-shot learning, the model is tested on several **N-way, K-shot classification** tasks. Each task involves the following steps:

1. **Task Setup**: For each episode, the model is presented with N classes (e.g., "star", "exoplanet", "background"), and for each class, K support images are sampled. A separate set of query images is also sampled for testing.

2. **Embedding Extraction**: The support and query images are passed through the ResNet18-based feature extractor, which converts each image into a 16-dimensional embedding.

3. **Prototype Calculation**: The model computes the prototypes for each of the N classes by averaging the embeddings of the support images.

4. **Query Classification**: The query embeddings are compared to the prototypes, and the class with the closest prototype is assigned as the predicted label.

5. **Metric Calculation**: After classification, metrics such as accuracy, precision, recall, and F1-score are calculated to evaluate the model's performance in the few-shot learning setting. These metrics are computed by comparing the predicted labels of the query images with their true labels.

Handling Limited Exoplanet Data

Given that labeled exoplanet data is rare, few-shot learning techniques such as Siamese Networks are invaluable. By relying on distance-based classification rather than large amounts of training data, the Siamese Networks enables the model to make accurate predictions about new exoplanets based on just a few labeled examples.
The shared embedding space (trained through contrastive learning) ensures that the model learns meaningful representations, which allows the Siamese Networks to distinguish between subtle differences in star and exoplanet images, even when data is limited. This is critical for effective exoplanet detection and classification in real-world astronomical datasets.

3.6 YOLOv5 for Localization of Stars and Exoplanets

YOLOv5 is a faster and precise deep learning architecture which is mainly employed in object detection techniques. The name YOLO stands for "You Only Look Once," emphasizing its key advantage: For comparison with YOLOv5, there are other object detection models that work on an image in stages or parts of the image while YOLOv5 3.8 only considers the whole image at initial level. This makes the model to be fast to deploy and capable of predicting not only the class of an object, but also its location, making it ideal for use in real-time applications. YOLOv5 3.8

operates through a predictive bounding box method; it boxes objects based on the grid nature it deploys on the image [23]. Prescribing where an object is located, these bounding boxes also predict what the object is, like a star, exoplanet, or another celestial body in the scope of our work. Every bounding box gives information about the position of the object on the picture, height, width, and even the output of the network that provides class probability to let YOLOv5 differentiate between the objects and give the details of what the object is. But one of the main aspects that make deep learning engineers choose YOLOv5 is that it offers high accuracy while having a high speed [23].

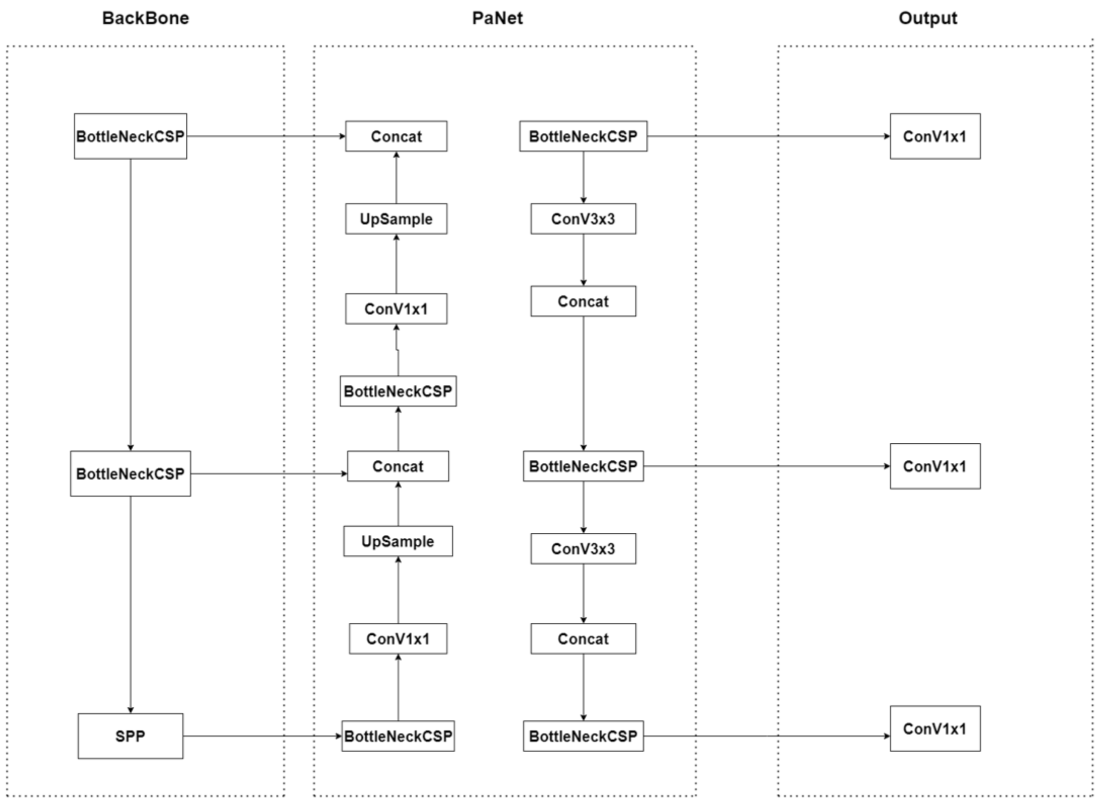

Figure 3.8: YOLOv5 Architecture

Despite fewer parameters and simpler operations, YOLOv5 maintains high speed and efficiency by processing entire images in a single pass, unlike models requiring multiple passes or region proposals. This speed is advantageous in projects with high data volumes or real-time requirements, such as astronomy applications for analyzing star or exoplanet images. YOLOv5 can detect multiple objects at once and identify multiple instances of the same object within an image, enhancing its efficiency. Its architecture has been optimized for both speed and accuracy, utilizing techniques like non-maximum suppression to reduce false positives and refine bounding boxes, making it well-suited for accurate, real-time detection in high-resolution imagery[23].

Where we are using YOLOv5 for the detection and localization of stars and exoplanets within the images captured by MIRI coronagraph in our project. The process of localization is critical as it does not only show where stars, or exoplanets, are but where they are situated in the picture. Concerning the position of these celestial bodies which YOLOv5 detects, it gets this right by providing the exact position of detected objects using these bounding boxes around them. Therefore, the choice of YOLOv5 is justified for our project because of its speed and effectiveness, with which it can analyze high-quality photographs obtained from MIRI coronagraphs. In contrast to the models that run successive passes or region proposals, YOLOv5 takes the entire image in one go and detects all the objects simultaneously. This approach means that large datasets can be negotiated more easily [23]. In addition, YOLOv5's accurate localization of coordinates is very useful in astronomy as we explain, since we are able to draw bounding boxes around stars and exoplanets allowing for a zoomed in look at the distinct characteristics of each celestial object. As well as, the multi-scale feature of YOLOv5 is effective for the detection of objects with different sizes and brightness, and it correctly detects both highly bright stars and low bright exoplanets within the same frame. These features allow for a significant increase in efficiency of effective analysis of a vast number of different astronomical processes.

3.7 YOLOv7 for Localization of Stars and Exoplanets

Originally designed for the problem of object detection in real-world scenarios, YOLOv7 can be beneficial for astronomer localization of both stars and exoplanets in telescope lens images. Compared to some prior applications, identifying astronomical sources necessitates conveying weakness and low contrast, and so researchers modify YOLOv7 accordingly. With these, one is to fine-tune the model with set weights in addition to using pre-processing techniques such as noise reduction , YOLOv7 3.9 becomes capable of precisely identifying distant stars and faint exoplanets even in dense star fields[30].

Improved for astronomy, YOLOv7 can address the small and closely associated objects seen in astronomy images. Both stars and exoplanets may be presented as point sources and seem faint; therefore, minor changes in the detection layers and thresholds will help to obtain better localization [30]. This optimised model amplifies contrasts and strikes out noises in complex space images making sure YOLOv7 does not skip on identifying objects up in space.

Overall, in the field of astronomy, the proposed method of YOLOv7 allows for fast detection and the determination of star clusters and the identification of new exoplanets in large datasets. An advantage of this approach is that it's real-time, thus enabling researchers in the analysis of astronomical images who needs time-sensitive data. In this particular context, YOLOv7 provides scientific literature contributions and usability within the field of space research.

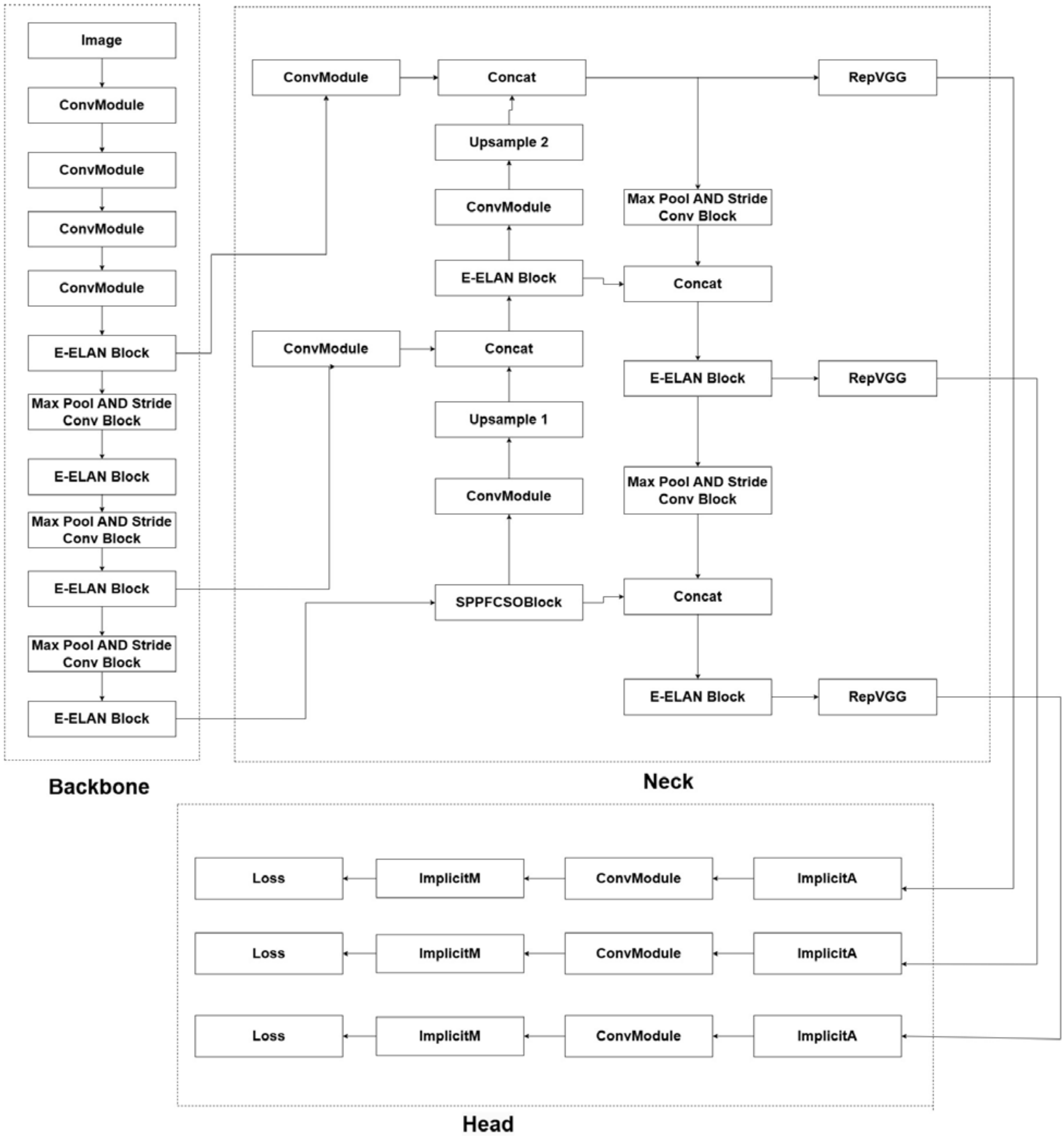

Figure 3.9: YOLOv7 Architecture

Chapter 4

Results and Discussion

4.1 Performance Metrics

This section evaluates the performance of the trained model used for exoplanet detection. Several key metrics have been used to assess the model's effectiveness, including accuracy, F1 score, precision, and recall. The results of the classification are visually represented using a confusion matrix, which provides a detailed breakdown of the model's predictions.

The confusion matrix summarizes the predictions of the exoplanet detection model by showing the counts of correct and incorrect classifications. This matrix is essential for understanding the model's strengths and weaknesses beyond simple accuracy. It breaks down the results into four metrics:

- **True Positive (TP):** Correctly identified exoplanets.
- **True Negative (TN):** Correctly identified stars.
- **False Positive (FP):** Stars that were incorrectly classified as exoplanets.
- **False Negative (FN):** Exoplanets that were missed and classified as stars.

The confusion matrix helps highlight where the model performs well and where improvements are needed, particularly in cases where classifying faint exoplanets could be challenging.

Recall, also known as sensitivity or the true positive rate, measures the model's ability to correctly identify all exoplanets. A high recall indicates that the model successfully captures most of the exoplanets in the dataset. In the context of exoplanet detection, a high recall is critical, as missing an exoplanet (false negatives) could mean missing key discoveries. However, increasing recall may sometimes lower precision, as more objects might be incorrectly classified as exoplanets.

$$\text{Recall} = \frac{TP}{TP + FN} \tag{1}$$

Precision measures how many of the objects predicted to be exoplanets are actually exoplanets. In other words, it reflects the accuracy of the positive predictions made by the model. In exoplanet detection, a higher precision ensures that false positives (misclassified stars) are minimized, which is important to avoid noise in the detection process.

$$\text{Precision} = \frac{TP}{TP + FP} \tag{2}$$

The F1 score is the harmonic mean of precision and recall, providing a balanced metric that considers both false positives and false negatives. For exoplanet detection, the F1 score is a useful metric to evaluate the trade-off between correctly identifying exoplanets and minimizing false alarms. A high F1 score indicates that the model is both accurate in detecting exoplanets and efficient in avoiding incorrect classifications.

$$\text{F1 Score} = 2 \times \frac{\text{Precision} \times \text{Recall}}{\text{Precision} + \text{Recall}} \tag{3}$$

Accuracy is the overall measure of how often the model makes correct predictions. It calculates the proportion of all correct predictions (both stars and exoplanets) out of the total number of predictions. While accuracy gives a general idea of model performance, it is important to consider it in conjunction with recall and precision, especially when dealing with imbalanced datasets like exoplanet detection, where the number of stars may vastly outnumber exoplanets.

$$\text{Accuracy} = \frac{TP + TN}{TP + TN + FP + FN} \times 100 \tag{4}$$

These performance metrics are critical for evaluating the model's success in exoplanet detection, allowing us to fine-tune the model based on specific needs such as higher recall for detecting all exoplanets or higher precision to avoid false positives.

4.2 Performance Evaluation of Exoplanet Detection Classification Based

4.2.1 Contrastive Learning with Siamese Network

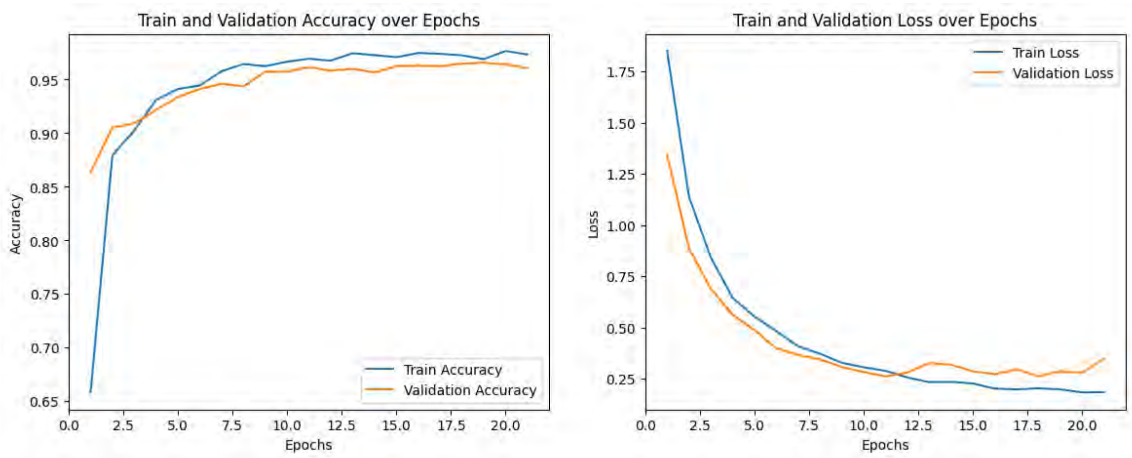

Figure 4.1: Line graph of Contrastive Learning and Siamese Network accuracy and loss

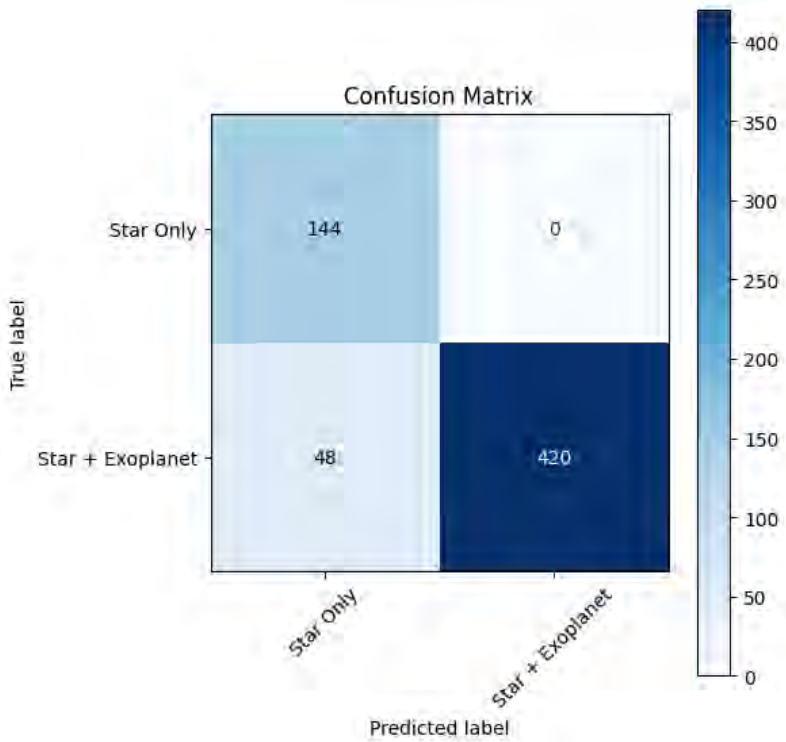

Figure 4.2: Confusion matrix graph of Contrastive Learning and Siamese Network.

The contrastive learning model integrated with a few-shot learning framework was assessed over a period of 25 epochs, but due to early stopping, it concluded training at the 20th epoch. By this point, the model achieved near-perfect results in both training and validation. In Figure 4.1, the training accuracy exhibits a steady improvement, beginning at approximately 65% and reaching close to 98% by the final epoch, while the training loss shows a consistent decline from an initial value of around 1.75 to nearly 0.1. This indicates effective model convergence and minimized errors during training. Similarly, validation accuracy rises in tandem with training accuracy, starting around 70% and achieving approximately 95% by epoch 20. Although validation loss initially decreases sharply, it eventually stabilizes and remains slightly above the training loss, reflecting the model's effectiveness in generalization. The final evaluation metrics reinforce this strong performance, with an accuracy of 92.16%, a perfect precision of 100.00%, recall of 89.74%, and an F1 score of 94.59%. These metrics indicate a balanced performance, demonstrating that the model is effective in identifying both the primary and contrasting classes accurately. The model effectively combined contrastive learning with few-shot learning to achieve high accuracy in both training and validation phases.

The model correctly classified 420 instances of the "Star + Exoplanet" class and 144 instances of the "Star Only" class, with only minor misclassifications. Specifically, 48 "Star + Exoplanet" instances were incorrectly predicted as "Star Only," while all "Star Only" instances were classified correctly, resulting in no false positives for this class. This confusion matrix, shown in Figure 4.2, illustrates the model's strong precision, particularly in detecting "Star Only" instances with no false positives. The combined use of contrastive learning with a Siamese network contributed to the model's high accuracy in both training and validation stages. It eventually stabilized above 90%, indicating good generalization to unseen data.The overall precision (100%) and recall (89.74%) reflect the model's effectiveness in minimizing false positives and false negatives, crucial in the domain of exoplanet detection.

4.2.2 MobileNetV2

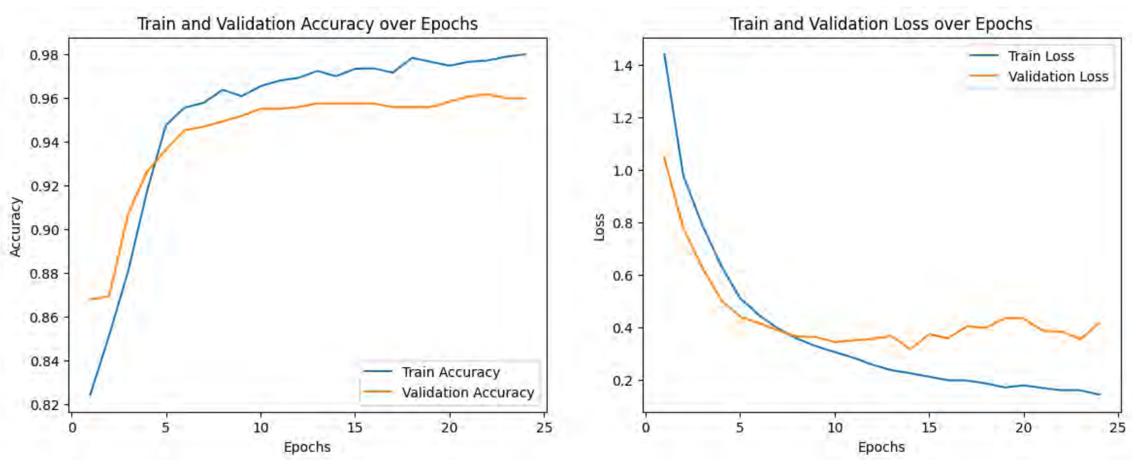

Figure 4.3: MobileNetV2 Accuracy and loss

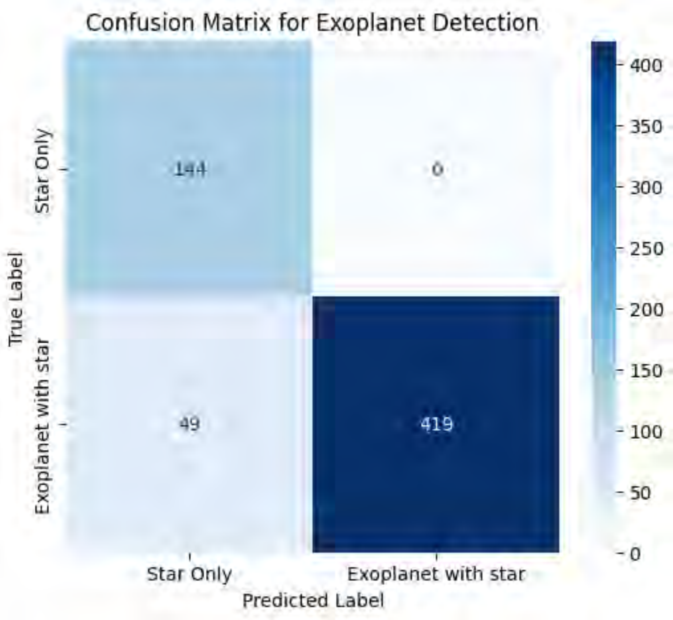

Figure 4.4: Confusion matrix of MobileNetV2

The pretrained MobileNetV2 model demonstrated effective performance in the exoplanet detection task. Over the course of 25 epochs, the model's accuracy showed a steady increase as it learned to distinguish between ”Star Only” and ”Exoplanet with Star.” In the initial epochs, both training and validation accuracy rose sharply, reflecting the model's rapid learning phase. As the training progressed, the accuracy gains gradually tapered off, indicating that the model was approaching its optimal performance. By around the 20th epoch, both training and validation accuracy stabilized, demonstrating minimal improvement thereafter. This steady accuracy progression throughout training ultimately led to a final accuracy of 91.99%, indicating the model's capacity to generalize well without overfitting.

In terms of loss, the MobileNetV2 model showed a continuous reduction in both training and validation loss, suggesting a smooth learning process. Initially, the training loss started at a high value of around 1.4 and consistently decreased over the epochs, reaching approximately 0.1 by the final epoch, reflecting effective optimization during each training step. Similarly, the validation loss followed a comparable trajectory, starting around 1.2 and dropping close to 0.3 by the last epoch. The close alignment between training and validation loss throughout the epochs highlights consistent performance on unseen data, indicating the model's ability to generalize without significant overfitting.

The confusion matrix further illustrated the MobileNetV2 model's classification capabilities. For the ”Star Only” category, the model accurately predicted 144 instances without any false positives, demonstrating perfect precision in identifying stars that lacked exoplanets and highlighting the model's strength in correctly recognizing stars when no exoplanet is present. In the ”Exoplanet with Star” category, the model correctly classified 419 instances as exoplanets with stars, although it misclassified 49 instances as ”Star Only.” These misclassifications reflect some limitations in recall for exoplanet detection, as 49 exoplanet cases were missed and incorrectly labeled as ”Star Only.” Despite these errors, the high number of correct classifications (419 out of 468 total exoplanet cases) demonstrates strong overall performance, especially in accurately identifying exoplanets when they are present. The relatively low misclassification rate suggests that, while there is room for improvement in recall for exoplanet detection, the model effectively distinguishes between stars with and without exoplanets, maintaining a high level of accuracy across both classes.

Overall, MobileNetV2 demonstrated strong accuracy and stability in its loss metrics, indicating its effectiveness for the exoplanet classification task. The model’s minimal misclassifications reflect robust learning, though some improvement in recall for exoplanet detection could further enhance its performance.

4.2.3 Custom CNN

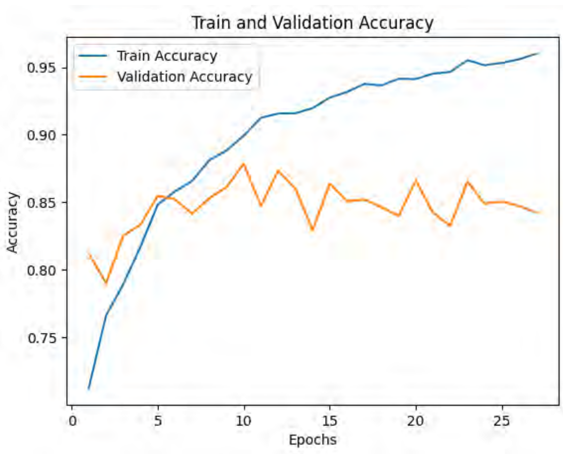

(a) Custom CNN Accuracy

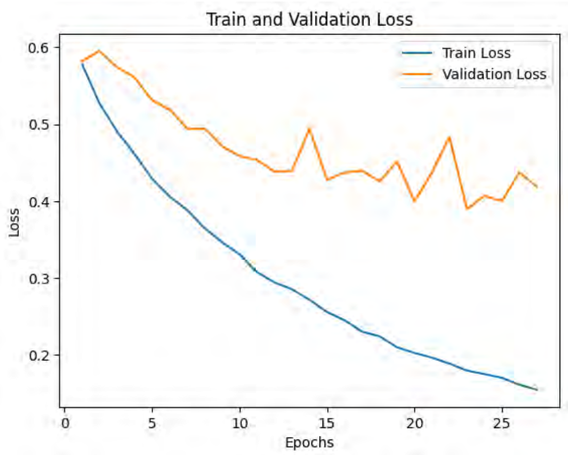

(b) Custom CNN Loss

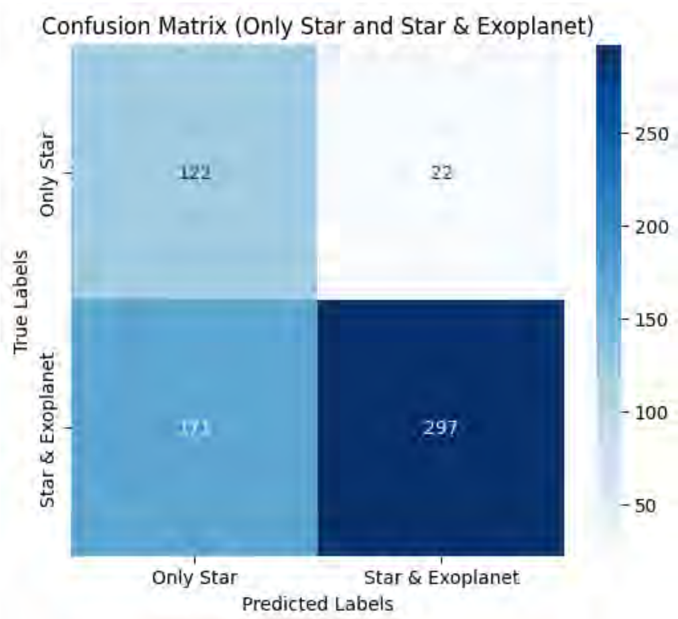

Figure 4.6: Confusion matrix of Custom CNN

The custom CNN model for exoplanet detection was trained over 30 epochs, with its performance evaluated on both training and validation datasets. Throughout the training process, the model exhibited steady improvement in training accuracy, starting at a lower baseline and gradually increasing to over 95% by the final epoch. Similarly, training loss displayed a consistent downward trend, beginning at a higher value and converging close to zero as the model learned to minimize errors effectively on the training data.
The validation accuracy, while initially rising, reached a plateau around 85% after the 10th epoch, suggesting that the model might be close to its generalization capacity on the validation set. Meanwhile, the validation loss demonstrated fluctuations, stabilizing around 0.4, which may indicate a mild overfitting trend. Despite this, the model maintained a balanced validation performance, reflecting reasonable generalization to unseen data. Final evaluation using the confusion matrix highlights the model's classification capabilities. Specifically:

- True Negatives (Stars correctly classified as Stars): 122
- False Positives (Stars misclassified as Exoplanets): 22
- False Negatives (Exoplanets misclassified as Stars): 171
- True Positives (Exoplanets correctly classified as Exoplanets): 297

From this data Accuracy of the model was approximately 68.5%, indicating that the model correctly classified about two-thirds of the total instances. Precision for Exoplanets stood at 93.1%, showing the model's high reliability when predicting exoplanets. Recall for Exoplanets was relatively lower at 63.5%, suggesting that the model missed a notable portion of actual exoplanet instances. Specificity for Stars was 84.7%, indicating the model's strong ability to correctly classify star instances. The confusion matrix reveals that while the model performs well in identifying exoplanets with high precision, it struggles with recall, as a significant number of exoplanets are misclassified as stars. This performance pattern suggests that the model is effective in minimizing false positives but could benefit from further tuning to reduce false negatives.
In summary, the custom CNN model achieved a strong balance between precision and specificity, particularly in identifying exoplanets. Although some overfitting signs are observed, the overall metrics indicate the model's effectiveness for exoplanet detection, with room for further optimization to enhance recall.

4.3 Comparative Study

As shown in Table 4.1, the Contrastive Learning with Siamese Network model demonstrated the strongest performance across all key metrics for both star and exoplanet detection. It achieved the highest accuracy of 92.16%, along with a perfect precision of 100%, indicating that it accurately identified all instances labeled as exoplanets. The model's recall was 89.74%, showing its capability to correctly detect nearly 90% of actual exoplanet cases, and its F1 score was 94.59%, reflecting a well-balanced trade-off between precision and recall.

In comparison, MobileNetV2 also exhibited strong performance, achieving an accuracy of 91.99% and a precision of 100%. However, its recall was slightly lower at 89.53%, leading to a comparable but marginally lower F1 score of 94.48%. Despite its high accuracy, the Siamese Network demonstrated a slight edge in recall and F1 score, suggesting a more balanced generalization across both classes.

On the other hand, the Custom CNN model showed significantly weaker performance, with an accuracy of 68.46% and a lower recall of 63.46%, underscoring its limitations in detecting exoplanets accurately. Although it achieved a precision of 93.10%, its F1 score of 75.48% reveals challenges in both accuracy and recall, particularly in exoplanet classification.

Overall, the Contrastive Learning with Siamese Network emerges as the top model for this task, consistently achieving the highest accuracy, balanced classification metrics, and effective generalization across both star and exoplanet classes. Its superior performance underlines its suitability for complex astronomical classification tasks, making it the most optimal choice among the models evaluated.

Table 4.1: Performance Comparison Classification Models

Model	**Accuracy**	**Precision**	**Recall**	**F1 Score**
Contrastive Learning with Siamese Network	**92.16%**	**100%**	**89.74%**	**94.59%**
MobileNetV2	91.99%	100%	89.53%	94.48%
Custom CNN	68.46%	93.10%	63.46%	75.48%

4.4 Comparative Study with YOLO classifier

The overall performance comparison in Table 4.2 demonstrates the exceptional capability of the Contrastive Learning model with a Siamese Network. This model achieved a precision of 100.00%, recall of 89.96%, and an F1 score of 94.71%, highlighting its effectiveness in accurately detecting and classifying both stars and exoplanets with minimal false positives and missed detections. The model also achieved an impressive accuracy of 92.32%, underscoring its reliability in this classification task.

The YOLOv5 model displayed moderate performance, achieving an accuracy of 90.24%, a precision of 93.60%, a recall of 91.20%, and an F1 score of 92.40%. Although its performance was reasonable, it did not reach the effectiveness of the Contrastive Learning model with Siamese Network.

The YOLOv7 model performed slightly better than YOLOv5, with an accuracy of 92.02%, a precision of 93.03%, a recall of 89.61%, and an F1 score of 91.11%. However, it still fell short when compared to the proposed Contrastive Learning model with Siamese Network, especially in precision and F1 score, where the proposed model demonstrated substantially higher values.

Overall,the Contrastive Learning with Siamese Network model outperformed both YOLOv5 and YOLOv7 across all metrics, establishing it as the most effective model for accurate detection and classification tasks related to stars and exoplanets.

Table 4.2: Overall Performance Comparison of Classification Models

Model	**Accuracy**	**Precision**	**Recall**	**F1 Score**
Contrastive Learning with Siamese Network	**92.32%**	**100%**	**89.96%**	**94.71%**
YOLOv5	90.24%	93.60%	91.20%	92.40%
YOLOv7	92.02%	93.03%	89.61%	91.11%

4.5 Performance Evaluation of Exoplanet and Star Detection

4.5.1 YOLOv5

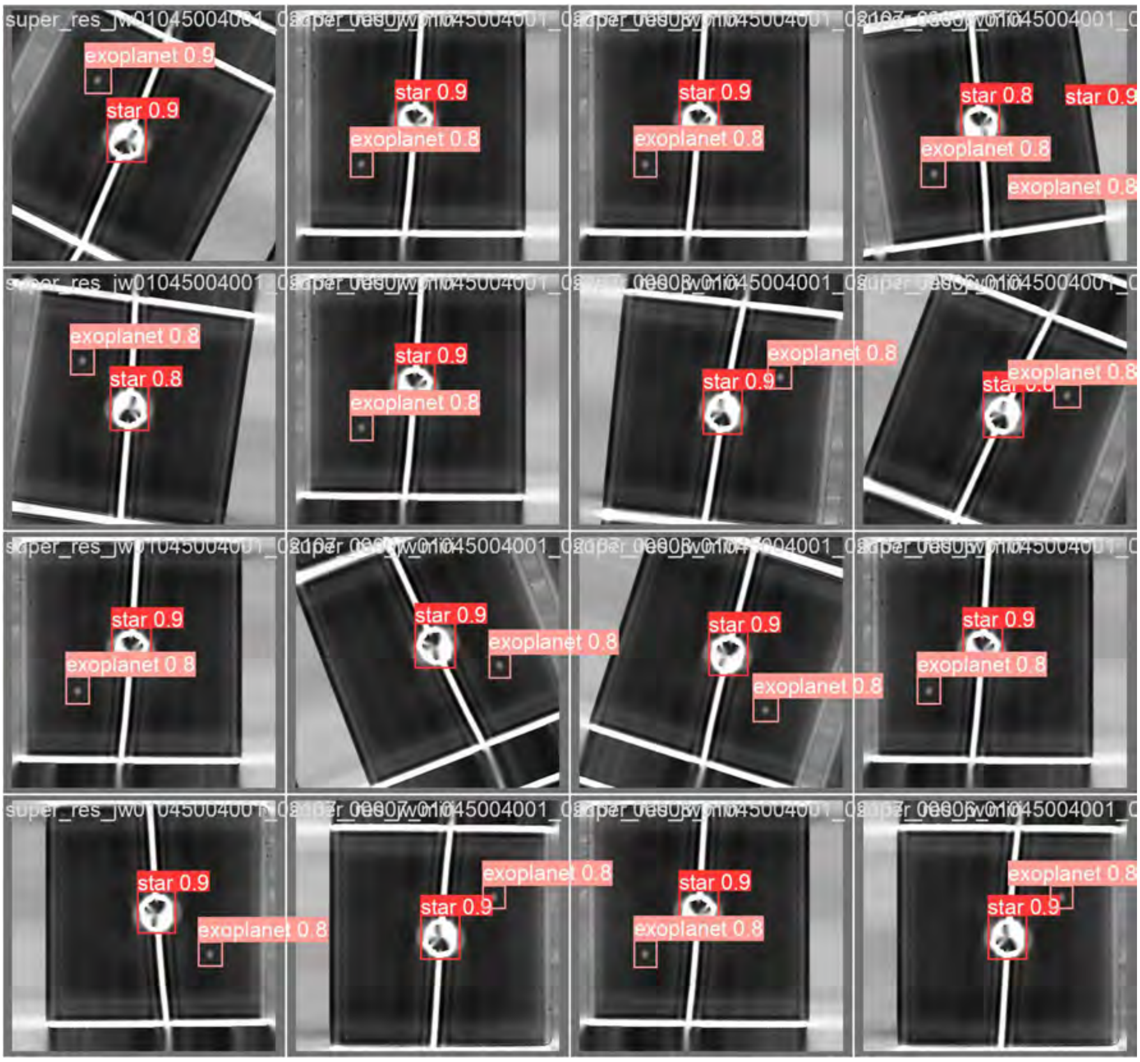

Figure 4.7: Predicted Output of Exoplanet and Star

In the predicted output figure in 4.7 both "exoplanet" and "star" objects are labeled with confidence scores. The "star" detections show a consistent confidence score of 0.9 across various orientations which demonstrates high certainty in identifying this class. Meanwhile the "exoplanet" detections are labeled with a confidence score of 0.8 showing slightly less certainty but still reliable predictions. This consistent labeling across multiple instances suggests a stable model performance in distinguishing and predicting both "star" and "exoplanet" objects in different positions and views within the dataset. The confusion matrix (Figure 4.8) and training loss and accuracy curves (Figure 4.9) illustrate the model's effectiveness in distinguishing between the two classes.

This confusion matrix (Figure 4.8) shows the classification performance for three classes: star, exoplanet, and background. Starting with the star class in the first row the model correctly predicted 0.98 of the true star instances as star. However it misclassified 0.02 of the true star instances as background and none as exoplanet. Moving to the second row which represents the true exoplanet instances the model accurately classified 0.94 as exoplanet. Nevertheless 0.06 of the true exoplanet instances were incorrectly classified as background and 0.34 were misclassified as background. In the third row which indicates the background class the model correctly identified 0.66 of the true background instances as background. Despite this it misclassified 0.34 of the background instances as exoplanet and none as star. Thus this matrix provides insight into both the correct predictions and misclassifications made by the model across the different classes.

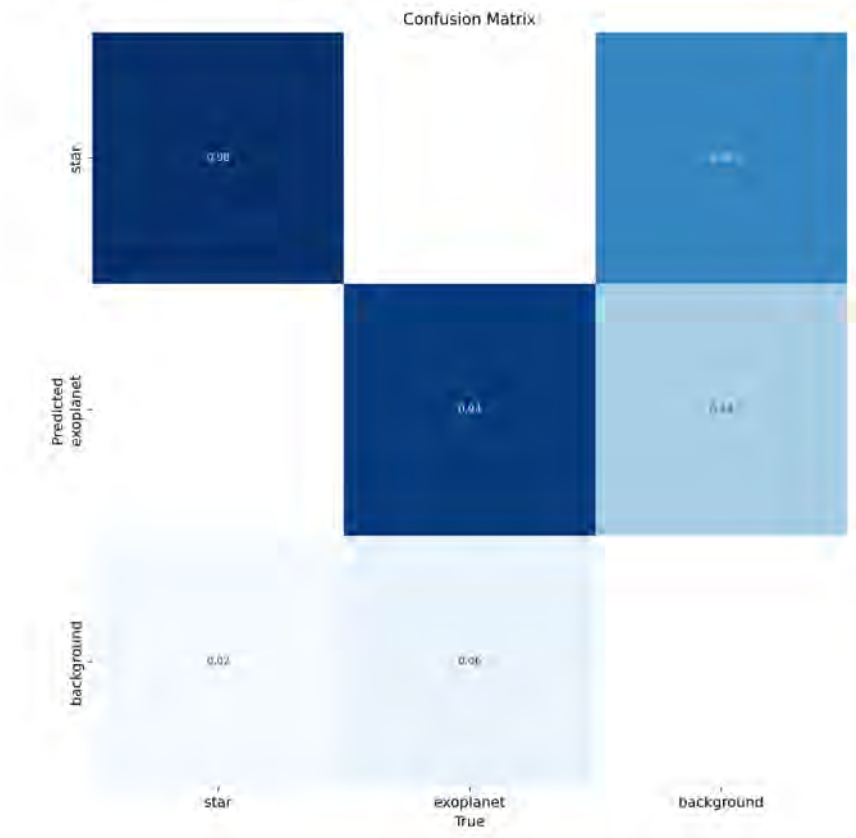

Figure 4.8: Confusion Matrix of Exoplanet with Star

The training and validation loss curves in Figure 4.9 along with various performance metrics over epochs are shown in this figure. Starting with the training loss curves we observe a decreasing trend for the box loss which starts at approximately 0.1 and steadily declines to around 0.02. The object loss also shows a similar downward trend beginning close to 0.025 and reaching around 0.01 by the end of the training. Additionally the classification loss for training decreases from around 0.025 to almost zero indicating improved model performance as training progresses.

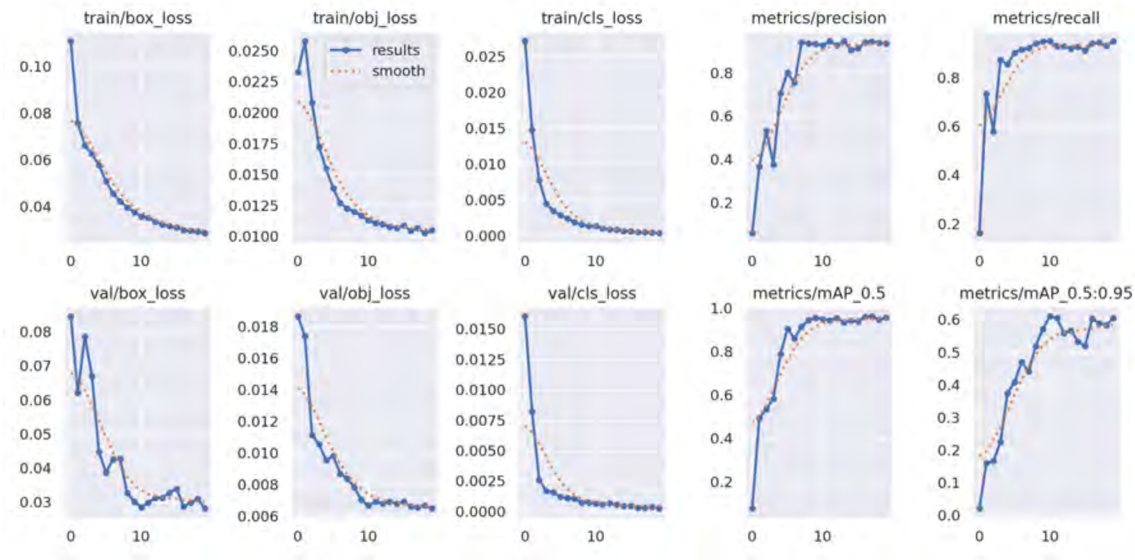

Figure 4.9: Loss curve and Performance Curve

In the validation loss curves a similar pattern emerges. The box loss begins at roughly 0.08 and reduces to about 0.03 by the last epoch. The object loss in validation shows a decrease from around 0.018 down to approximately 0.006. Furthermore the classification loss for validation begins at about 0.015 and drops close to zero indicating the model's consistent performance across both training and validation. The precision metric shows an upward trend stabilizing above 0.8 by the later epochs reflecting improved accuracy in the model's predictions. Similarly recall increases over time and reaches around 0.9 indicating better detection rates as training progresses. The metric mAP@0.5 which represents mean Average Precision at IoU threshold 0.5 shows an increase that stabilizes above 0.8 by the end. Finally the metric mAP@0.5:0.95 representing mean Average Precision across multiple IoU thresholds shows improvement over epochs stabilizing around 0.6 indicating balanced performance across various IoU values. Overall these curves show that the model's losses decrease while precision recall and mean Average Precision metrics improve consistently through training.

The figure 4.10 presents two bar graphs that display the Dice coefficient and Intersection over Union (IoU) values for two classes: Star and Exoplanet. In the Dice coefficient graph on the left we observe that the Star class achieves a Dice coefficient of 1.0 indicating a perfect overlap between predicted and true areas. Meanwhile the Exoplanet class has a slightly lower Dice coefficient close to 0.9 which suggests a high but not perfect overlap.

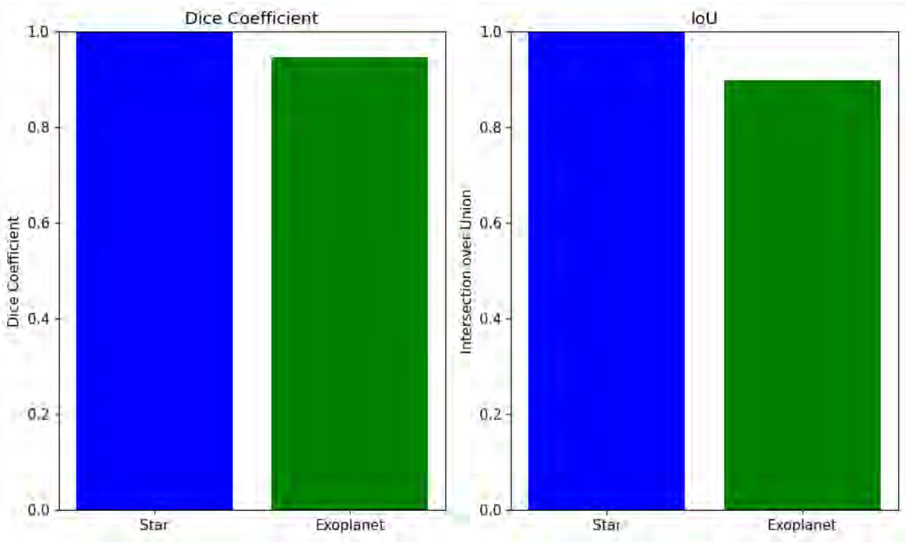

Figure 4.10: Dice coefficient and IoU OF YOLOv5

On the right side the IoU graph shows similar results. The Star class reaches an IoU of 1.0 indicating complete intersection with the true area. For the Exoplanet class the IoU is slightly less than 0.9 which reflects a minor discrepancy between predicted and actual regions. Altogether these graphs indicate that the model performs exceptionally well for the Star class while showing strong but slightly less accurate results for the Exoplanet class.

Overall,this study demonstrates the effectiveness of a YOLOv5-based model in detecting and segmenting stars and exoplanets. With high Dice coefficients and IoU values, the model shows near-perfect performance for stars and strong accuracy for exoplanets. Training and validation metrics illustrate consistent improvements, with decreasing losses and increasing precision, recall, and mean Average Precision.

4.5.2 YOLOv7

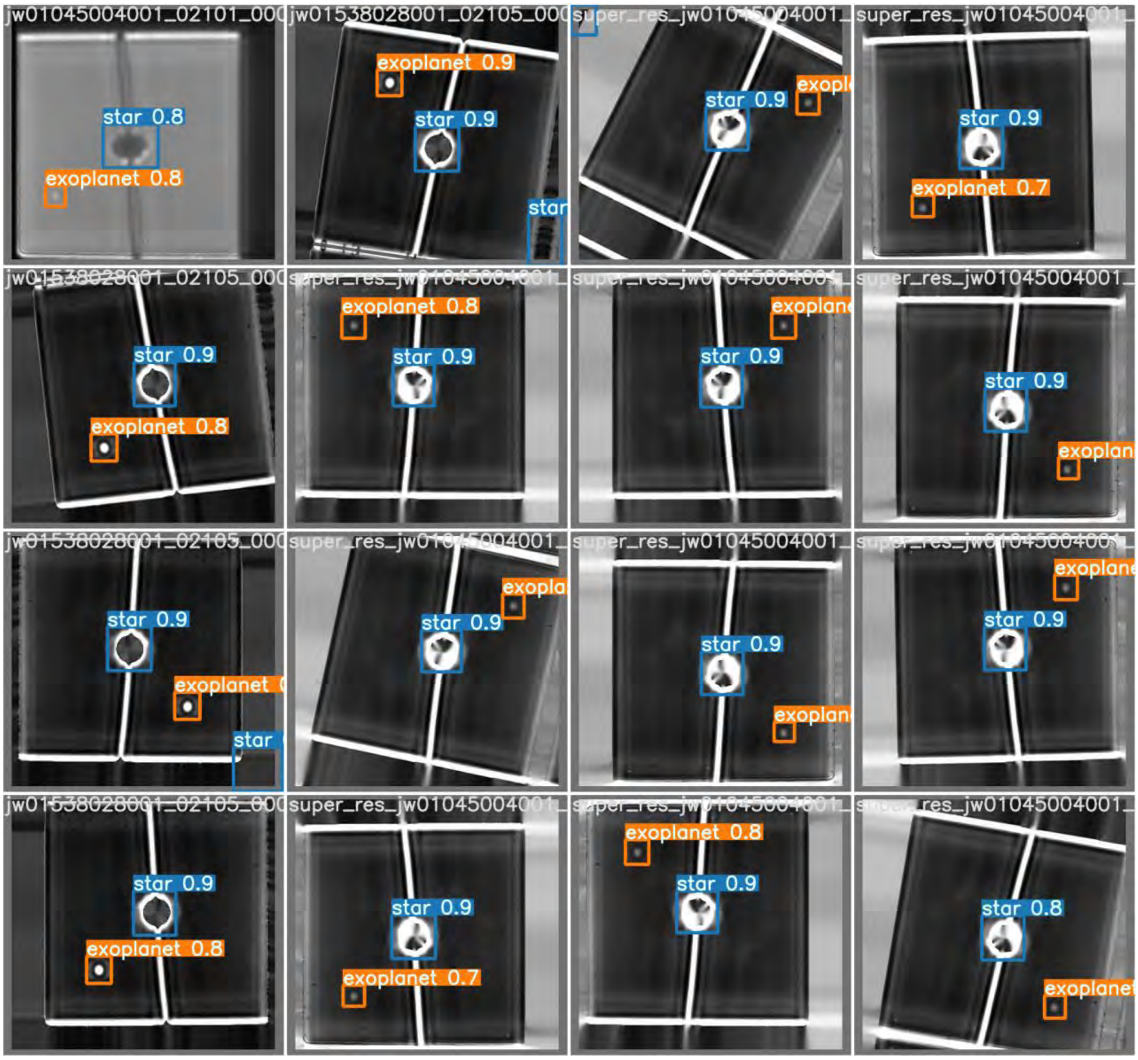

Figure 4.11: Predicted Output of Exoplanet and Star

The confusion matrix in Figure 4.12 provides a detailed analysis of the YOLOv7 model's performance in distinguishing between two classes: star and exoplanet. Each cell in the matrix represents the model's classification accuracy for these categories, revealing insights into its ability to correctly identify these celestial objects. The model shows a high true positive rate for both classes. For stars, it correctly identifies instances with a 97% accuracy, indicating that the model is highly confident in recognizing stars. This strong performance suggests that the model has effectively learned distinctive features that allow it to accurately differentiate stars from other classes. Similarly, the exoplanet class achieves a true positive rate of 84%, which reflects the model's capability in identifying exoplanets. However, the presence of misclassifications indicates challenges, particularly in distinguishing between background noise and actual celestial objects.

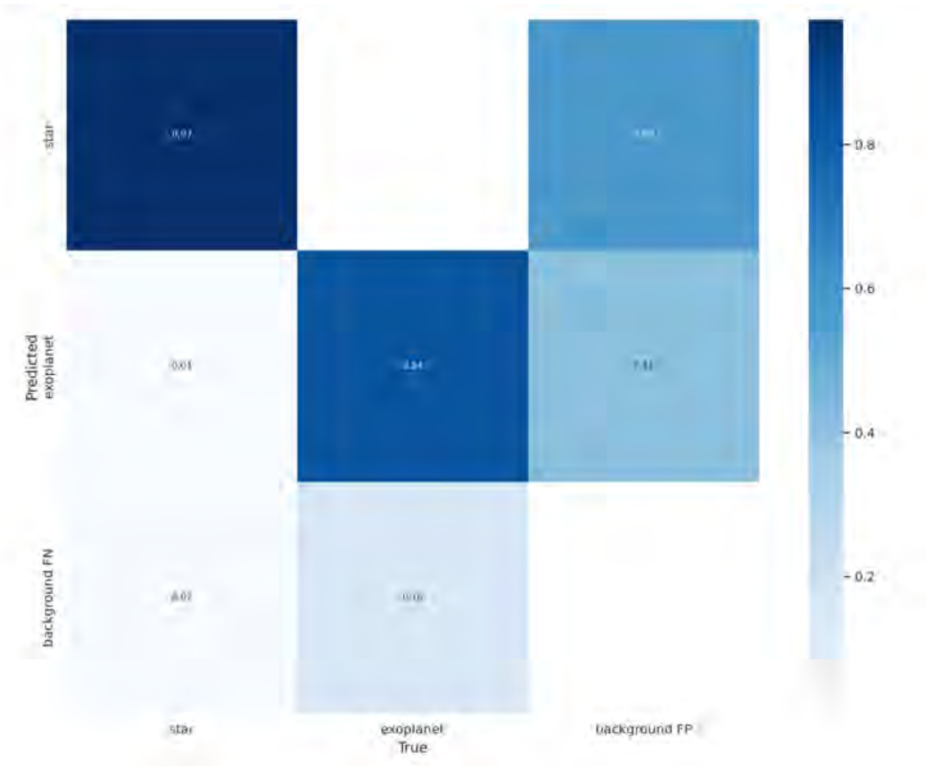

Figure 4.12: Confusion Matrix of Exoplanet with Star

Additionally, Figure 4.13 presents the training process, showing a steady decline in the training loss curves, which include box, objectness, and classification losses. This trend indicates effective learning and convergence over time. However, fluctuations in the validation loss, particularly in "val Box," "val Objectness," and "val Classification" losses, suggest some difficulties in maintaining generalization across different validation sets.
Figure 4.14 illustrates the Dice coefficient and Intersection over Union (IoU) values for both classes, further highlighting the model's segmentation and detection accuracy. For the star class, the model achieves a Dice coefficient of 0.94 and an IoU of 0.89, reflecting strong accuracy in recognizing and segmenting star objects. For the exoplanet class, the Dice coefficient is slightly lower at 0.88, with an IoU of 0.78. These values indicate the model's relative proficiency in detecting stars while facing greater challenges with exoplanets. The lower IoU and Dice scores for exoplanets suggest that the model may struggle to capture the boundaries of exoplanets as accurately as it does for stars.

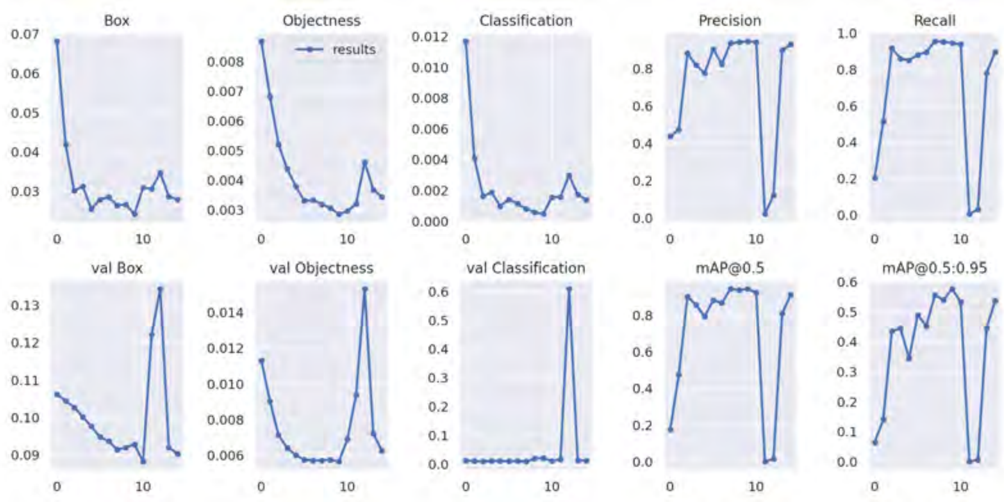

Figure 4.13: Loss curve and Performance Curve

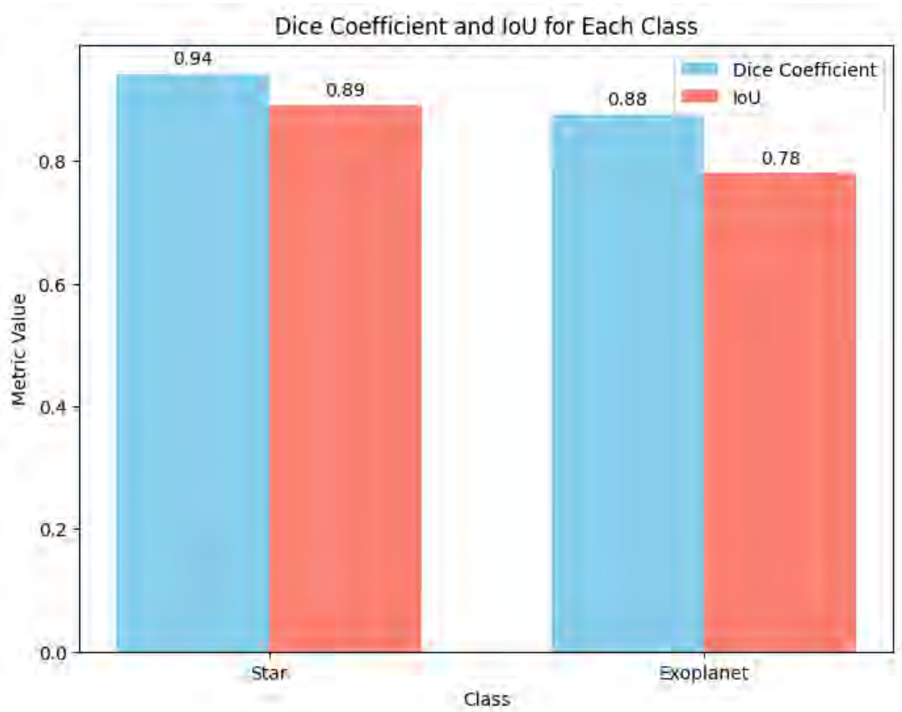

Figure 4.14: YOLOv7 Dice Coefficient

YOLOv7, with approximately 40 layers, 36.9 million parameters, and 104.7 GFLOPs, provides an architecture that balances accuracy and computational efficiency. During validation on a set of 612 images, the model achieved a precision of 0.9 and recall of 0.88, indicating high detection accuracy. The mAP@0.5 metric reached approximately 0.92, while mAP@0.5:0.95 was 0.55. This performance highlights the model's ability to distinguish between stars, exoplanets, and background, achieving a balanced precision and recall while maintaining segmentation accuracy, as indicated by the Dice coefficient and IoU values.

4.6 Comparative Study

In the figure 4.10, which illustrates the results of the YOLOv5 model, the Dice Coefficient and Intersection over Union (IoU) metrics are shown separately for two classes: "Star" and "Exoplanet." The Dice Coefficient for the "Star" class is close to 1.0, indicating nearly perfect overlap between the predicted and actual masks. However, the Dice Coefficient for "Exoplanet" is slightly lower, suggesting a small but noticeable difference. Similarly, the IoU for the "Star" class is also near 1.0, while the "Exoplanet" class has a slightly lower IoU value. These metrics indicate that YOLOv5 performs very well for the "Star" class but shows a small drop in performance for the "Exoplanet" class.

The figure 4.14, representing the results of the YOLOv7 model, provides a side-by-side comparison of the Dice Coefficient and IoU values for both classes. For the "Star" class, the Dice Coefficient is 0.94 and the IoU is 0.89, indicating strong performance but slightly less accuracy compared to YOLOv5. For the "Exoplanet" class, the Dice Coefficient is 0.88, and the IoU is 0.78. While YOLOv7 demonstrates consistent performance across both classes, it has slightly lower values than YOLOv5, suggesting it may not be as effective in precisely segmenting these classes.

Overall, YOLOv5 outperforms YOLOv7 in terms of both Dice Coefficient and IoU for the "Star" and "Exoplanet" classes. YOLOv5 achieves higher accuracy, especially for the "Star" class, and maintains a small advantage for the "Exoplanet" class. Therefore, YOLOv5 appears to be the better model in this context, as it provides more accurate segmentation results across the evaluated classes.

Chapter 5

Conclusion

In conclusion, this thesis demonstrates the potential of leveraging contrastive learning and few-shot learning for exoplanet detection in direct imaging. While modern instruments like JWST and MIRI coronagraph have provided high-quality datasets, traditional methods struggle with the challenges of faint exoplanets and small, imbalanced datasets. The proposed framework, which integrates contrastive learning with ResNet18 and Siamese Networks, addresses these challenges by learning robust representations that separate celestial objects amidst noise and low contrast. Furthermore, the application of few-shot learning enables effective detection with limited pixel-labeled data. This approach provides improved accuracy over simpler methods, demonstrating its potential for advancing direct imaging exoplanet identification and paving the way for future astronomical discoveries.

While the research showed promising results, several limitations impacted the model's scope and performance. The primary challenge was limited access to large-scale annotated datasets, which, despite the use of few-shot learning, constrained model generalization. Access to more diverse datasets would likely improve outcomes. Additionally, the computational demands of processing astronomical imagery, such as converting raw FITS files to PNGs, led to some potential loss of information, even with techniques like median filtering and contrast enhancement. These preprocessing steps may have affected the model's ability to capture subtle features. Furthermore, time constraints significantly limited extensive hyperparameter tuning and longer training periods, both of which could have enhanced model optimization, particularly for complex models like SimCLR, MoCo, and Prototypical Networks. Transfer learning using ResNet18 mitigated some of these challenges, but longer training and better computational resources would have likely improved results.

5.1 Future Works

The outcomes of this research pave the way for several potential future research directions:

1. **Incorporating Larger Datasets:** Expanding the dataset to include more diverse planetary systems could improve the model's robustness and accuracy. Collaboration with astronomical institutions for access to larger datasets from projects like Gaia and TESS would be beneficial.

2. **Exploring Other Contrastive Learning Models:** In future work, additional contrastive learning models, such as CLIP and BYOL, can be tested to compare their performance with the ones used in this study. These models may provide even more effective feature embeddings, which could enhance classification performance in the few-shot learning setting.

3. **Multimodal Learning:** The integration of multiple data modalities (e.g., combining imaging with light curve data) could provide a richer feature space for training the models, leading to better detection of exoplanets that may not be visible in images alone.

This study highlights the potential of using machine learning to tackle some of the most challenging tasks in astronomy, but continued research is needed to address these limitations and build upon the findings.

Bibliography

[1] G. Christie, “Detecting exoplanets by gravitational microlensing using a small telescope,” no. 21, Oct. 2006. [Online]. Available: https://www.researchgate.net/publication/1790129.

[2] A. Zakharov, S. Novati, F. De Paolis, G. Ingrosso, P. Jetzer, and A. Nucita, “Exoplanet searches with gravitational microlensing,” no. 20, Jan. 2010. [Online]. Available: https://www.researchgate.net/publication/228636832_Exoplanet_searches_with_gravitational_microlensing.

[3] L. Shannon, D. Russell, and R. Campbell, “Exoplanet transits: Light curve photometry,” *Center for Astrophysics Space Physics and Engineering Research at Baylor University*, no. 5, Jul. 2012, Observations of three separate exoplanet transits using flatfield and dark image processing to create light curves and estimate exoplanet properties.

[4] J. Wright and B. Gaudi, “Exoplanet detection methods,” *Planets, Stars and Stellar Systems. Volume 3: Solar and Stellar Planetary Systems*, Oct. 2012. DOI: 10.1007/978-90-481-8818-5_59.

[5] A. Cassan, “Extrasolar planets detections and statistics through gravitational microlensing,” no. 21, Oct. 2014. [Online]. Available: https://www.researchgate.net/publication/281989184_Extrasolar_planets_detections_and_statistics_through_gravitational_microlensing.

[6] Ž. Ivezić, A. J. Connolly, J. Vanderplas, and A. Gray, “Statistics, data mining, and machine learning in astronomy,” 2014. [Online]. Available: https://api.semanticscholar.org/CorpusID:60402728.

[7] P. Plavchan, D. Latham, *et al.*, “Radial velocity prospects current and future – a white paper report prepared by the study analysis group 8 for the exoplanet program analysis group (exopag),” *arXiv*, vol. 1503.01770, Mar. 2015. DOI: 10.48550/arXiv.1503.01770.

[8] L. Lindegren, U. Lammers, U. Bastian, J. I. G. Hern’andez, S. A. Klioner, D. Hobbs, A. Bombrun, D. Michalik, M. Ramos-Lerate, A. G. Butkevich, G. Comoretto, E. Joliet, and B. Holl, “Gaia data release 1 - astrometry: One billion positions, two million proper motions and parallaxes,” *Astronomy and Astrophysics*, vol. 595, 2016. [Online]. Available: https://api.semanticscholar.org/CorpusID:8382743.

[9] C. Gomez Gonzalez, O. Absil, and M. Droogenbroeck, “Supervised detection of exoplanets in high-contrast imaging sequences,” *Astronomy Astrophysics*, vol. 613, Dec. 2017. DOI: 10.1051/0004-6361/201731961.

[10] B. J. Fulton, E. A. Petigura, S. Blunt, and E. Sinukoff, "Radvel: The radial velocity modeling toolkit," *Publications of the Astronomical Society of the Pacific*, vol. 130, no. 986, pp. 1–13, Apr. 2018. DOI: 10.1088/1538-3873.

[11] I. Goodfellow, "Generative adversarial networks," *arXiv:1812.03664*, 2018. arXiv: 1812.03664 [cs.LG]. [Online]. Available: https://arxiv.org/abs/1812.03664.

[12] N. Schanche, A. C. Cameron, G. Hébrard, L. Nielsen, A. H. M. J. Triaud, J. M. Almenara, K. A. Alsubai, D. R. Anderson, D. J. Armstrong, S. C. C. Barros, F. Bouchy, P. Boumis, D. J. A. Brown, F. Faedi, K. Hay, L. Hebb, F. Kiefer, L. Mancini, P. F. L. Maxted, E. Palle, D. L. Pollacco, D. Queloz, B. Smalley, S. Udry, R. West, and P. J. Wheatley, "Machine-learning approaches to exoplanet transit detection and candidate validation in wide-field ground-based surveys," *Monthly Notices of the Royal Astronomical Society*, vol. 483, no. 3, pp. 5534–5547, Nov. 2018, ISSN: 1365-2966. DOI: 10.1093/mnras/sty3146. [Online]. Available: http://dx.doi.org/10.1093/mnras/sty3146.

[13] Y. Tsapras, "Microlensing searches for exoplanets," *Geosciences*, vol. 8, no. 19, p. 365, Sep. 2018. DOI: 10.3390/geosciences8100365. [Online]. Available: https://www.researchgate.net/publication/328035964_Microlensing_Searches_for_Exoplanets.

[14] ——, "Microlensing searches for exoplanets," *Geosciences*, vol. 8, no. 10, p. 365, 2018, ISSN: 2076-3263. DOI: 10.3390/geosciences8100365. [Online]. Available: http://dx.doi.org/10.3390/geosciences8100365.

[15] D. Baron, "Machine learning in astronomy: A practical overview," *arXiv: Instrumentation and Methods for Astrophysics*, 2019. [Online]. Available: https://api.semanticscholar.org/CorpusID:119302873.

[16] P. Chintarungruangchai and I.-G. Jiang, "Detecting exoplanet transits through machine-learning techniques with convolutional neural networks," *Publications of the Astronomical Society of the Pacific*, vol. 131, no. 4, pp. 1–15, 2019, ISSN: 00046280, 15383873. [Online]. Available: https://www.jstor.org/stable/26660768 (visited on 01/24/2024).

[17] T. Chen, S. Kornblith, M. Norouzi, and G. Hinton, "Simclr: A simple framework for contrastive learning of visual representations," *arXiv:2002.05709*, 2020. arXiv: 2002.05709 [cs.LG]. [Online]. Available: https://arxiv.org/pdf/2002.05709.

[18] M. Jara-Maldonado, V. Alarcon-Aquino, R. Rosas-Romero, O. Starostenko, and J. Ramirez-Cortes, "Transiting exoplanet discovery using machine learning techniques: A survey," *Earth Science Informatics*, no. 2, Sep. 2020. DOI: 10.1007/s12145-020-00464-7.

[19] P. H. Le-Khac, G. Healy, and A. F. Smeaton, "Contrastive representation learning: A framework and review," *IEEE Access*, vol. 8, pp. 193 907–193 934, 2020. DOI: 10.1109/ACCESS.2020.3031549.

[20] K. H. Yip, N. Nikolaou, P. Coronica, A. Tsiaras, B. Edwards, Q. Changeat, M. Morvan, B. Biller, S. Hinkley, J. Salmond, M. Archer, P. Sumption, E. Choquet, R. Soummer, L. Pueyo, and I. P. Waldmann, "Pushing the limits of exoplanet discovery via direct imaging with deep learning," in *Lecture Notes in Computer Science*. Springer International Publishing, 2020, pp. 322–338, ISBN: 9783030461331. DOI: 10.1007/978-3-030-46133-1_20. [Online]. Available: http://dx.doi.org/10.1007/978-3-030-46133-1_20.

[21] A. Malik, B. P. Moster, and C. Obermeier, "Exoplanet detection using machine learning," *Monthly Notices of the Royal Astronomical Society*, no. 1, Dec. 2021, ISSN: 1365-2966. DOI: 10.1093/mnras/stab3692. [Online]. Available: http://dx.doi.org/10.1093/mnras/stab3692.

[22] B. Schölkopf, F. Locatello, S. Bauer, N. R. Ke, N. Kalchbrenner, A. Goyal, and Y. Bengio, "Toward causal representation learning," *Machine Learning*, vol. 110, no. 9, pp. 2765–2798, 2021. DOI: 10.1007/s10994-020-05917-0. [Online]. Available: https://link.springer.com/article/10.1007/s10994-020-05917-0.

[23] R. Kaur and S. Singh, "A comprehensive review of object detection with deep learning," *Journal of Computer Science Review*, 2022. [Online]. Available: https://www.sciencedirect.com/topics/computer-science/yolov5.

[24] A. K. Kembhavi and R. Pattnaik, "Machine learning in astronomy," *Journal of Astrophysics and Astronomy*, vol. 43, pp. 1–10, 2022. [Online]. Available: https://api.semanticscholar.org/CorpusID:252905569.

[25] T. Müller, G. Pérez-Torró, and M. Franco-Salvador, "Few-shot learning with siamese networks and label tuning," *arXiv preprint arXiv:2203.14655*, 2022.

[26] D. Nardiello, L. R. Bedin, A. J. Burgasser, M. Salaris, S. Cassisi, M. Griggio, and M. Scalco, "Photometry and astrometry with jwst – i. nircam point spread functions and the first jwst colour-magnitude diagrams of a globular cluster," 2022. [Online]. Available: https://api.semanticscholar.org/CorpusID:252222289.

[27] J. V. Rodríguez, I. Rodríguez-Rodríguez, and W. L. Woo, "On the application of machine learning in astronomy and astrophysics: A text-mining-based scientometric analysis," *Wiley Interdisciplinary Reviews: Data Mining and Knowledge Discovery*, vol. 12, 2022. [Online]. Available: https://api.semanticscholar.org/CorpusID:251559919.

[28] Z. Ahmed, S. D'Amico, R. Hu, and M. Damiano, "Exoplanet detection from starshade images using convolutional neural networks," in *Proceedings of the SPIE*, Stanford University and Jet Propulsion Laboratory, California Institute of Technology, 2023.

[29] O. Flasseur, T. Bodrito, J. Mairal, J. Ponce, M. Langlois, and A.-M. Lagrange, "Deep paco: Combining statistical models with deep learning for exoplanet detection and characterization in direct imaging at high contrast," *Monthly Notices of the Royal Astronomical Society*, Oct. 2023.

[30] S. M. John, F. A. Kareem, S. G. Paul, A. G. M, S. Al Mansoori, and A. Panthakkan, “Enhanced yolov7 model for accurate vehicle detection from uav imagery,” *2023 International Conference on Innovations in Engineering and Technology (ICIET)*, pp. 1–4, 2023. DOI: 10.1109/ICIET57285.2023.10220850.

[31] Q. Liang, M.-X. Lin, M. Trodden, and S. S. C. Wong, “Probing parity violation in the stochastic gravitational wave background with astrometry,” 2023. [Online]. Available: https://api.semanticscholar.org/CorpusID:263134390.

[32] G. K. Pandey and S. Srivastava, “Resnet-18 comparative analysis of various activation functions for image classification,” *International Conference on Inventive Computation Technologies (ICICT)*, pp. 595–601, 2023. DOI: 10.1109/ICICT57646.2023.10134464.

[33] J. E. Wenskovitch and A. D. Jaodand, “Human factors for machine learning in astronomy,” *Human Factors and Simulation*, 2023. [Online]. Available: https://api.semanticscholar.org/CorpusID:259711188.

[34] AstroImageJ Team, *Astroimagej: Image processing software*, https://www.astro.louisville.edu/software/astroimagej/, Accessed: 2024-10-17, 2024.

[35] CVAT Team, *Computer vision annotation tool (cvat)*, https://www.cvat.ai/, Accessed: 2024-10-17, 2024.

[36] European Space Agency, *Jwst science archive*, Accessed: 2024-10-17, 2024. [Online]. Available: https://jwst.esac.esa.int/archive/#search.

[37] Mikulski Archive for Space Telescopes, *Mast portal*, Accessed: 2024-10-17, 2024. [Online]. Available: https://mast.stsci.edu/portal/Mashup/Clients/Mast/Portal.html.

[38] G. Nath-Ranga, P. Patapis, H. Hoeijmakers, and S. Quanz, “Machine learning for exoplanet detection in high-contrast spectroscopy,” *arXiv preprint arXiv:2405.13469*, 2024. arXiv: 2405.13469 `[astro-ph.IM]`. [Online]. Available: https://ar5iv.labs.arxiv.org/html/2405.13469.